

THRESHOLD SELECTION AND TRIMMING IN EXTREMES

MARTIN BLADT (corresponding author)

*Department of Actuarial Science, Faculty of Business and Economics,
University of Lausanne, CH-1015 Lausanne, Switzerland*

HANSJÖRG ALBRECHER

*Department of Actuarial Science, Faculty of Business and Economics and Swiss
Finance Institute, University of Lausanne, CH-1015 Lausanne, Switzerland*

JAN BEIRLANT

*Department of Mathematics, KU Leuven, Celestijnenlaan 200B, B-3001
Leuven, Belgium, and Department of Mathematical Statistics and Actuarial
Science, University of the Free State, South Africa*

ABSTRACT. We consider removing lower order statistics from the classical Hill estimator in extreme value statistics, and compensating for it by rescaling the remaining terms. Trajectories of these trimmed statistics as a function of the extent of trimming turn out to be quite flat near the optimal threshold value. For the regularly varying case, the classical threshold selection problem in tail estimation is then revisited, both visually via trimmed Hill plots and, for the Hall class, also mathematically via minimizing the expected empirical variance. This leads to a simple threshold selection procedure for the classical Hill estimator which circumvents the estimation of some of the tail characteristics, a problem which is usually the bottleneck in threshold selection. As a by-product, we derive an alternative estimator of the tail index, which assigns more weight to large observations, and works particularly well for relatively lighter tails. A simple ratio statistic routine is suggested to evaluate the goodness of the implied selection of the threshold. We illustrate the favourable performance and the potential of the proposed method with simulation studies and real insurance data.

1. INTRODUCTION

The use of Pareto-type tails has been shown to be important in different areas of risk management, such as for instance in computer science, insurance and finance. In social sciences and linguistics the model is referred to as Zipf's law.

E-mail addresses: martin.bladt@unil.ch, hansjoerg.albrecher@unil.ch,
jan.beirlant@kuleuven.be.

Date: June 30, 2020.

This model corresponds to the max-domain of attraction of a generalized extreme value distribution with a positive extreme value index (EVI) ξ :

$$(1) \quad 1 - F(x) = x^{-1/\xi} \ell(x), \quad \xi > 0,$$

where ℓ denotes a slowly varying function at infinity:

$$(2) \quad \lim_{x \rightarrow \infty} \frac{\ell(ux)}{\ell(x)} = 1, \text{ for every } u > 0.$$

Since the appearance of the paper of Hill (1975) in which the EVI estimator

$$(3) \quad H_{k,n} = \frac{1}{k} \sum_{i=1}^k \log X_{n-i+1,n} - \log X_{n-k,n}$$

was proposed with

$$X_{n,n} \geq X_{n-1,n} \geq \cdots \geq X_{n-i+1,n} \geq \cdots \geq X_{1,n}$$

denoting the ordered statistics of a random sample from F , the literature on estimation of $\xi > 0$ and other tail quantities such as extreme quantiles and tail probabilities has increased exponentially. We refer to Embrechts et al. (2013), Beirlant et al. (2004), de Haan and Ferreira (2007) and Gomes and Guillou (2015) for detailed discussions and reviews of these estimation problems. Next to the proposal of numerous estimators, focus has gradually shifted to selection methods of k and to the construction of bias-reduced estimators which exhibit plots of estimates which, as a function of k , are as stable as possible. Indeed, plots of estimators of ξ as a function of k that are consistent under the large semi-parametric model (1) are hard to interpret. In case of the Hill estimator some authors refer to Hill horror plots. While it has been frequently suggested to choose a 'stable' area (see for instance Drees et al. (2000) and De Sousa and Michailidis (2004)), such a stable part is often absent or hard to find. Sometimes more than one stable section is present, like in some insurance applications as we will discuss later.

The typical available guidelines for the choice of k to be used in the implementation of the EVI estimators depend strongly on the properties of the tail itself, and k needs to be estimated adaptively from the data. This problem can be compared with choosing a bandwidth parameter in density estimation. It is typically suggested that the optimal value of k should be the one that minimizes the mean-squared error (MSE). However, this optimum depends on the sample size, the unknown value of ξ as well as on the nature of the slowly varying function ℓ , as was first described in Hall et al. (1985). Bootstrap methods were proposed in Hall (1990), Draisma et al. (1999), Danielsson et al. (2001), and Gomes and Oliveira (2001). Beirlant et al. (1996, 2002) derived regression diagnostic methods on a Pareto quantile plot. Other selection procedures can be found in Drees and Kaufmann (1998) and Guillou and Hall (2001). Possible heuristic choices are provided in Gomes and Pestana (2007), Gomes et al. (2008) and Beirlant et al. (2011). Recent proposals rooted in goodness-of-fit approaches are found in Bader et al. (2018), Drees et al. (2020) and Schneider et al. (2019). Almost all

authors consider the adaptive choice of k for the Hill estimator.

In this paper we consider trimming of the Hill estimator, omitting some of the lower order statistics in $X_{n-k+1,n}, \dots, X_{n,n}$, which leads to statistics of the type

$$(4) \quad T_{b,k} = \sum_{i=1}^b c_i(b, k) \log \left(\frac{X_{n-i+1,n}}{X_{n-k,n}} \right),$$

for some $1 \leq b \leq k$ and suitable constants $c_i(b, k)$. This kind of kernel-type statistics have been previously proposed (cf. Csörgő et al. (1985)) as estimators of ξ . However, the implementation of the optimal kernel is not an easy task nor our focus in this paper. Instead, we propose a special form of the kernel that leads to an identity which aids in the threshold estimation problem. In Section 2 we derive the coefficients $c_i(b, k)$ which make $T_{b,k}$ unbiased when ℓ is constant and when we force the coefficients $c_i(b, k) = c(b, k)$ not to depend on i . We present a novel lower-trimmed Hill plot which provides significant graphical support for the estimation problem of ξ , as we illustrate with both simulations and real world data. We also provide mathematical evidence that, as a function of b , the variability of the $T_{b,k}$ statistics is lower than the one in the Hill plot. In Section 3, we examine the asymptotic characteristics of $T_{b,k}$ in (4) under the general model (1). The asymptotic expected empirical variance of $T_{b,k}$ is shown to be less sensitive on the tail parameter ξ than the asymptotic mean-squared error (AMSE) of the usual Hill estimator (3). We identify a link between the corresponding two optimal k -choices which allows to bypass the specification of ξ and other characteristics of the tail behavior for the identification of the optimal threshold in the classical Hill estimate, and the resulting procedure turns out to be simple to implement in practice. Subsequently, we study the estimator \bar{T}_k obtained by averaging the trimmed Hill estimators over $b = 1, \dots, k$. This latter estimator naturally assigns more weight to the larger observations, the weights being only moderately changed when increasing k . Furthermore, the specification of these weights is independent of the distribution F . Note that, in contrast, earlier criteria for reweighting terms in the Hill estimator (such as e.g. Csörgő et al. (1985) in terms of kernel estimates, see also (Beirlant et al., 2002, Sec.3)) had to heavily rely on the tail parameter ξ . In Section 4 we then present a simple ratio statistic as a tool to evaluate the goodness of selection of k . Section 5 confirms the good performance of the proposed methods using simulations, where \bar{T}_k turns out to outperform the classical Hill estimator in almost all cases. Note that our approach eventually suggests a fully automated procedure for the threshold selection, also in the absence of knowledge about, or assumptions on, the tail characteristics. Section 6 favorably illustrates this on a set of real-life motor third party liability insurance data. We would like to emphasize that the approach proposed in this paper suggests a general procedure that can in principle also be applied to other estimators in extreme value analysis.

2. A LOWER-TRIMMED HILL STATISTIC

2.1. Derivation. Assume first, for simplicity, that we have independent and identically distributed (i.i.d.) exact Pareto random variables, X_1, X_2, \dots, X_n ,

with tail given by

$$(5) \quad \bar{F}(x) = (x/\sigma)^{-1/\xi}, \quad x \geq \sigma, \quad \xi, \sigma > 0,$$

and we are interested in robust estimation of the tail index ξ .

A main tool used throughout the paper is the well-known *Rényi representation*, which states (in the second distribution equality below), that for the order statistics of a random sample X_1, \dots, X_n from the distribution (5), one has, for $k \leq n$, with $Y_{i,k} = X_{n-i+1,n}/X_{n-k,n}$ ($i = 1, \dots, k$),

$$(6) \quad (\log(Y_{1,k}), \dots, \log(Y_{k,k})) \stackrel{d}{=} (E_{k,k}, \dots, E_{1,k}) \stackrel{d}{=} \left(\sum_{j=1}^k \frac{E_j^*}{k-j+1}, \dots, \frac{E_1^*}{k} \right).$$

Here, $E_{k,k} \geq \dots \geq E_{1,k}$ are the order statistics of an independent i.i.d. exponential sample E_1, \dots, E_k with mean ξ , and E_1^*, \dots, E_k^* is another independent i.i.d. exponential sample with mean ξ .

Bhattacharya et al. (2019) recently proposed linear estimators of the form

$$\hat{\xi}_{k_0,k} = \sum_{i=k_0+1}^k c_{k_0,k}(i) \log(Y_{i,k}), \quad 0 \leq k_0 < k < n,$$

in order to trim the upper order statistics in outlier-contaminated samples, where the constants $c_{k_0,k}(i)$ are chosen in a way to ensure that the resulting estimator for ξ is unbiased. For fixed k_0, k , the problem can then be recast into that of finding suitable weights δ_i such that one can write

$$\hat{\xi}_{k_0,k} = \sum_{i=k_0+1}^k c_{k_0,k}(i) E_{k-i+1,k} = \sum_{i=1}^{k-k_0} \delta_i E_{i,k}.$$

Using the Rényi representation (6) and solving some elementary linear equations, they derived $\delta_i = \frac{1}{r}$, $i < r$, and $\delta_r = (k-r+1)/r$. This led them to the so-called *trimmed Hill estimator*

$$\hat{\xi}_{k_0,k} = \frac{k_0+1}{k-k_0} \log(Y_{k_0+1,k}) + \frac{1}{k-k_0} \sum_{i=k_0+2}^k \log(Y_{i,k}),$$

which is shown to be quite useful in outlier detection under (1).

In a similar way, but for a different purpose, in this paper we investigate trimming from the left. Concretely, we consider estimators of the form

$$T_{b,k} = \sum_{i=1}^b c_i(b,k) \log(Y_{i,k}), \quad 0 < b \leq k,$$

where $c_i(b,k)$ are constants to be determined. As above, we would like to find suitable weights γ_i such that

$$(7) \quad T_{b,k} = \sum_{i=1}^b c_i(b,k) E_{k-i+1,k} = \sum_{i=k-b+1}^k \gamma_i E_{i,k}$$

Setting $q = k - b + 1$, the Rényi representation (6) yields

$$\begin{aligned} T_{b,k} &= \sum_{i=q}^k \gamma_i E_{i,k} = \sum_{i=q}^k \gamma_i \sum_{j=1}^i \frac{E_j^*}{k-j+1} \\ &= \sum_{j=1}^k E_j^* \sum_{i=j \vee q}^k \frac{\gamma_i}{k-j+1} = \sum_{j=1}^k \bar{\gamma}_j E_j^* \end{aligned}$$

with $\bar{\gamma}_j := \sum_{i=j \vee q}^k \frac{\gamma_i}{k-j+1}$. Here we use the notation $j \vee q = \max\{j, q\}$. Unfortunately, the set of equations

$$\bar{\gamma}_j = \frac{1}{k}, \quad j = 1, \dots, k,$$

has no solution (for $j \leq q$ the left-hand-side cannot remain constant in j). Instead, we choose to set

$$(8) \quad \gamma_q = \gamma_{q+1} = \dots = \gamma_k =: \frac{1}{\bar{\omega}(q, k)}$$

and

$$(9) \quad \mathbb{E}[T_{b,k}] = \xi$$

as the defining equations. The solution of (8) and (9) is given by

$$(10) \quad \bar{\omega}(q, k) = \sum_{j=1}^k \frac{k - j \vee q + 1}{k - j + 1}.$$

Plugging (10) into (7), we then arrive at the following definition of a *lower-trimmed Hill statistic* $T_{b,k}$:

$$\begin{aligned} T_{b,k} &= \sum_{i=q}^k \frac{\log(Y_{k-i+1,k})}{\bar{\omega}(q, k)} = \frac{\sum_{i=1}^b \log(Y_{i,k})}{\bar{\omega}(k-b+1, k)} \\ (11) \quad &= \frac{\frac{1}{b} \sum_{i=1}^b \log(Y_{i,k})}{1 + \sum_{j=b+1}^k j^{-1}}, \quad b = 1, \dots, k, \quad k < n, \end{aligned}$$

where we use the convention $\sum_{j=k+1}^k j^{-1} := 0$.

Note that $T_{b,k}$ can be considered as a trimmed pseudo-likelihood estimator of ξ under the strict Pareto model (5). Indeed, under (5) the exceedances $Y_{i,k}$ ($i = 1, \dots, k$) are distributed as the order statistics from a sample of size k from (5) with $\sigma = 1$. Then the trimmed likelihood, considering the conditioning on the exceedances larger than $Y_{b+1,k}$, is given by

$$\prod_{i=1}^b \left(\frac{1}{\xi} Y_{i,k}^{-1/\xi-1} \right) / Y_{b+1,k}^{-1/\xi},$$

leading to the likelihood equation

$$(12) \quad \frac{1}{\xi} \frac{1}{b} \sum_{i=1}^b \log Y_{i,k} = 1 + \log Y_{b+1,k}^{1/\xi}.$$

From (6) it follows that $\mathbb{E}(\log Y_{b+1,k}^{1/\xi}) = \sum_{j=b+1}^k j^{-1}$, from which the estimator $T_{b,k}$ follows after formal substitution of $\log Y_{b+1,k}^{1/\xi}$ by its expected value in (12).

2.2. A lower-trimmed Hill plot. The so-called Hill plots, in which $T_{k,k}$ are plotted as a function of k , probably are the most popular starting tool in extreme value analysis for Pareto-type tails. However, the difficulties involved when interpreting these plots and searching for 'horizontal' or 'stable' parts that indicate the start of a tail part that resembles a pure Pareto tail, if at all available, constitute a serious obstacle in practical applications. In the literature, two lines of research have been developed in order to remedy these problems: adaptive selection of k along some criteria such as minimization of the MSE, or bias-reduction searching for estimators that are more stable, hence reducing the drift due to bias when k is taken too large. Concerning the line of research on bias reduction we can refer to recent papers using ridge regression methods in Buitendag et al. (2019) or Mean-of-Order- p estimators from Gomes et al. (2016), and the many other proposals cited in those papers. Both approaches, adaptive selection and bias reduction, can provide extra insight in a given case and complement each other. For instance, with increasing k bias-reduced estimators often start deviating from the original Hill plot at or around MSE-optimal k levels. Moreover, next to the selection of an appropriate threshold, stable bias-reduced methods based on extended Pareto models can provide models that fit well on a larger set of top data, see for instance Papastathopoulos and Tawn (2013) and the references therein.

While in the next sections we propose an adaptive selection method for k , we also suggest plotting $T_{b,k}$ defined above for $b = 1, \dots, k$ and different k , as it is unbiased for any b, k , $b \leq k$ under (5) by construction. Analogous to the Hill plot, we exploit the second degree of freedom and plot, for selected values of k , $T_{b,k}$ as a function of b . That is, the plot is constructed by overlaying the trajectories

$$(b, T_{b,k}), \quad b = 1, \dots, k,$$

for a selection of k values. The lower variance of these trajectories, comes from the fact that the normalizing order statistic is fixed, and hence a non-constant behaviour is easier to identify visually than in the classical Hill plot. As a particular consequence, the selection of k that makes the tail resemble a pure Pareto tail is easier to determine, by examining when the trajectories start to be constant, and hence indicating zones with reduced bias.

The following Proposition provides mathematical evidence for the above observations.

Proposition 2.1. *As a function of the number b of order statistics being used, in the exact Pareto case (5) the estimator $T_{b,k}$ has lower variance than the classical*

Hill estimator $T_{b,b}$. More precisely,

$$\mathbb{V}[T_{b,b}] = \frac{\xi^2}{b} \quad \text{and} \quad \mathbb{V}[T_{b,k}] \leq \frac{\xi^2}{\sum_{j=1}^{k-b+1} \left(\frac{b}{k-j+1}\right)^2 + b}.$$

As an illustration, we now compare the performance of these lower-trimmed Hill (LTH) plots for Pareto, near-Pareto and spliced Pareto distributions. The latter is defined through its cumulative distribution function (c.d.f.)

$$(13) \quad F(x; \xi_0, r, c) = \frac{(1 - x^{-1/\xi_0 - r} \mathbf{1}\{x \geq c\}) - 1\{x \geq c\}(c^{-1/\xi_0} - c^{-1/\xi_0 - r})}{1 - c^{-1/\xi_0} + c^{-1/\xi_0 - r}}, \quad x \geq 1$$

for $c \geq 1$ and $r > -1/\xi_0$, which is the c.d.f. of a Pareto random variable with tail index ξ_0 up to some splicing point c , continuously pasted with the c.d.f. of a Pareto random variable with another tail index $\xi = (1/\xi_0 + r)^{-1}$ thereafter. Splicing models (also sometimes referred to as composite models) are for instance popular in reinsurance modelling, cf. (Albrecher et al., 2017, Ch.4).

Concretely we simulated a sample of size $n = 1000$ from a:

- pure Pareto $\xi = \sigma = 1$ sample, defined in (5).
- spliced Pareto sample, defined in (13), with parameters $\xi = 1$, $\xi_0 = 1/4$ and splicing point $c = 1.3$.
- Student-t distribution with 10 degrees of freedom. The absolute value function was applied to the sample.
- Burr sample with tail $\bar{F}(x) = \left(\frac{1}{1+x}\right)^5$, $x > 0$ (which amounts to a generalized Pareto distribution).
- Log-gamma with logshape parameter $3/2$ and lograte parameter 1, i.e. with density $f(x) = \frac{1}{\Gamma(3/2)} (\log x)^{1/2} x^{-2}$, $x > 0$, with $\xi = 1$.

The LTH plots together with usual Hill plots are shown in the top panels of Figures 1–5. Reduced-bias plots based on Mean-of-Order- p_0 estimators are added in Figures 2–5. We restrict here to $p_0 = -1$ (different choices were also considered, but did not yield substantial differences). The LTH plots are made for a selection of k , from 1 to 1000 by spacings of 50 (1,51,101,...), as a function of the lower trimming b . Recall that $b \leq k$, so the lines have different domains on the x-axis. Observe that the right end-point of each of the overlaid lines corresponds to the respective point in the Hill plot. The bottom panels of Figures 1–5 suggest two ways of measuring the aforementioned flatness of the LTH estimator as a function of b . The first one computes the empirical variance of $T_{b,k}$, $b = 1, \dots, k$, while the second one fits a linear model with independent variable $b = 1, \dots, k$ and response variable $T_{b,k}$, and then plots the magnitude of the resulting slope coefficient.

For the spliced distribution in Figure 2 observe how the LTH estimator becomes horizontal as a function of b when k is close to the (rank of the) splicing point. For smaller k , the plot then looks similar to the exact Pareto case. Loosely speaking, the slope of the lines are a useful visual tool for detecting the number of upper order statistics k after which a Pareto tail is feasible. The case of the Student-t (Figure 3) and Burr (Figure 4) distribution show the problem of a large bias for the Hill estimator throughout, where the regime of a Pareto tail is only reached at the most extreme quantiles, and stable k areas are not really available. The Hill plot is roughly a monotone function of the number of order statistics, while the bias-reduced estimator already departs from the Hill plot at small values of k . The k levels indicated by the LTH variance and slope plots confirms that conclusion. Finally, the log-gamma distribution (Figure 5) with a logarithmic slowly varying function is known to be a difficult case for extreme value analysis: the Hill plot does show a stable area up to k around 500, where the estimates still exhibit a large bias. The reduced-bias estimates follow the Hill estimates for most of the plot up to k around 500, and this range is also indicated by the LTH slope plot.

In the next sections we will develop inferential and data-driven selection and estimation tools on the basis of these graphical tools.

3. REGULARLY VARYING TAILS

We now move from the simple Pareto sample to a general Fréchet domain of attraction, with tails of the form (1). Denote by Q the quantile function associated to F , and define

$$U(x) = Q(1 - 1/x), \quad x > 1,$$

such that the condition (1) is equivalent to

$$\lim_{t \rightarrow \infty} \frac{U(tx)}{U(t)} = x^\xi.$$

Assumptions on the rate of convergence of the above limit make it possible to obtain explicit results concerning asymptotic properties of the lower-trimmed Hill estimator. Hence, we impose the second order condition

$$(14) \quad \lim_{t \rightarrow \infty} \frac{\log U(tx) - \log U(t) - \xi \log(x)}{Q_0(t)} = \frac{x^p - 1}{p},$$

for some regularly varying function Q_0 with index $p < 0$.

Theorem 3.1. *Under the model (1) and second order condition (14), $T_{b,k}$ as defined in (11) satisfies the following asymptotic distributional identity, for $n, k, n/k \rightarrow \infty$,*

$$(15) \quad T_{b,k} \stackrel{d}{=} \xi \frac{\bar{E}_b + \sum_{j=b+1}^k E_j/j}{1 + \sum_{j=b+1}^k j^{-1}} + \frac{Q_0(n/k)}{p} \frac{\frac{((k+1)/b)^p - 1}{1-p} - 1}{1 + \sum_{j=b+1}^k j^{-1}} (1 + o_p(1)),$$

where E_1, \dots, E_k are i.i.d. standard exponential random variables, and where we use the notation $\bar{E}_b = b^{-1} \sum_{i=1}^b E_i$.

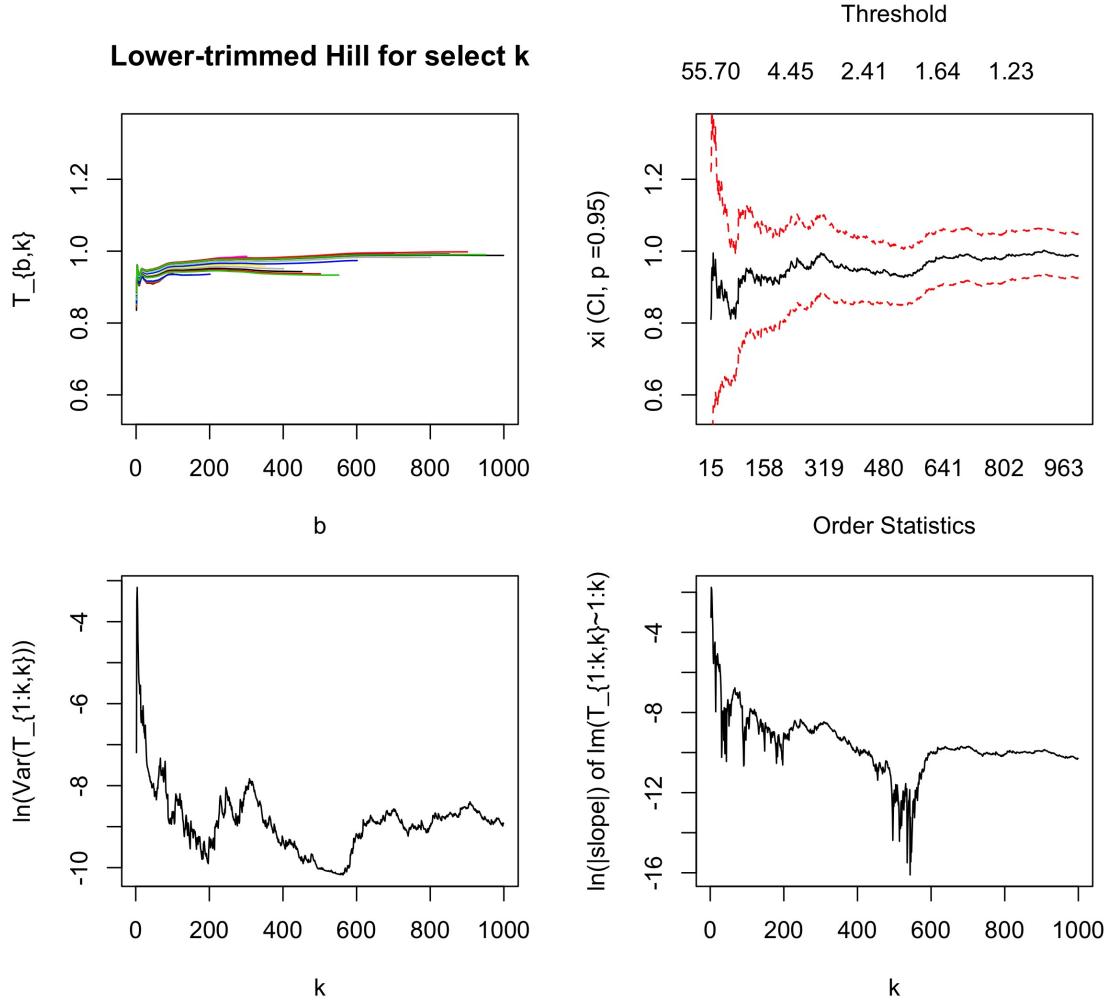


FIGURE 1. Exact Pareto case ($\xi = 1$). Top left: $T_{b,k}$ for varying lower trimming b , for $k = 1, 51, 101, \dots, 1000$. Top right: Hill plot (black, solid). Bottom left: empirical variance of the LTH as a function of k . Bottom right: slope of a fitted linear model to the LTH as a function of k .

3.1. **Distribution of the average.** Define the average of the $T_{b,k}$ across b as

$$(16) \quad \bar{T}_k := \frac{1}{k} \sum_{b=1}^k T_{b,k},$$

which by Theorem 3.1 satisfies

$$\bar{T}_k \stackrel{d}{=} \frac{\xi}{k} \sum_{b=1}^k \frac{\bar{E}_b + \sum_{j=b+1}^k E_j/j}{1 + \sum_{j=b+1}^k j^{-1}} + \frac{Q_0(n/k)}{pk} \sum_{b=1}^k \frac{\frac{((k+1)/b)^p - 1}{1-p}}{1 + \sum_{j=b+1}^k j^{-1}} (1 + o_p(1)).$$

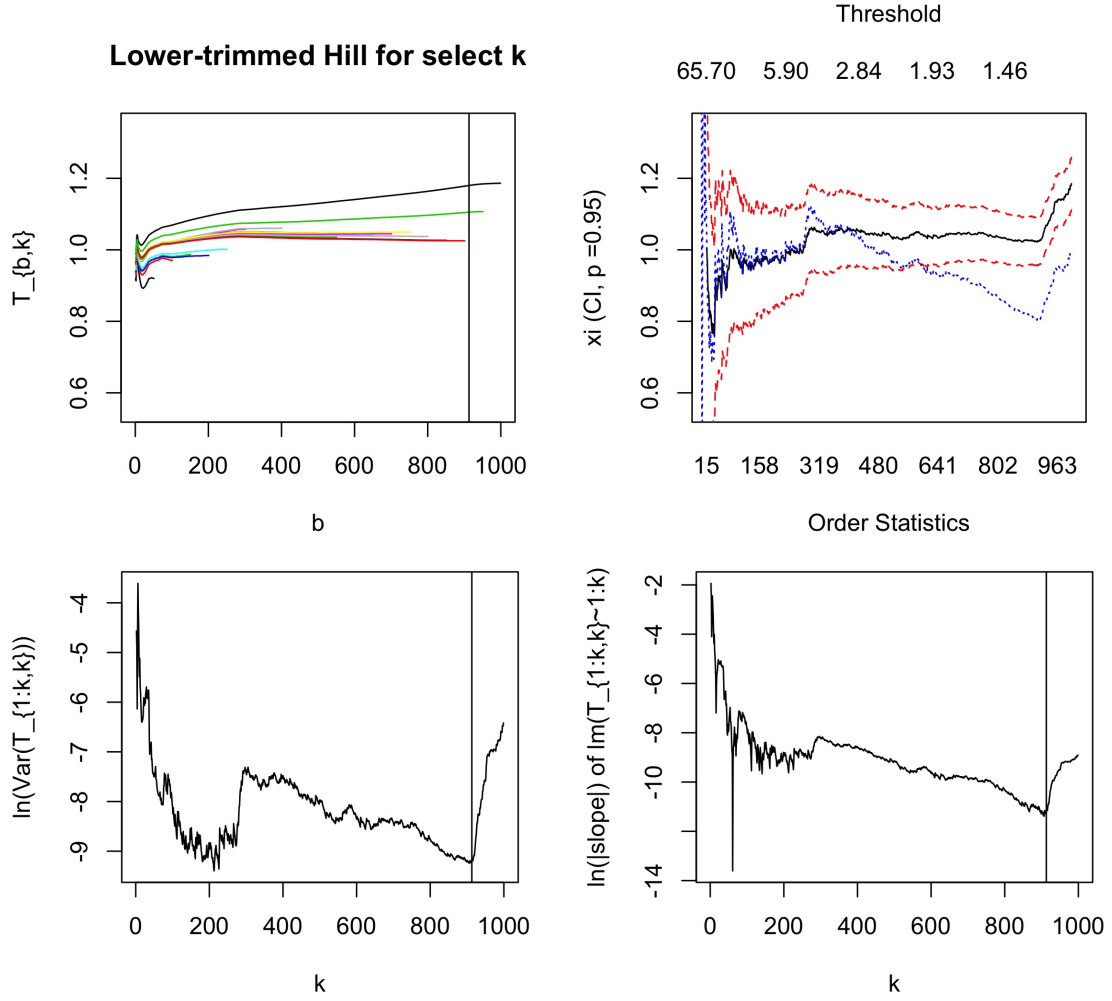


FIGURE 2. Spliced Pareto case (body parameter: $1/4$ and tail parameter: 1). Top left: $T_{b,k}$ for varying lower trimming b , for $k = 1, 51, 101, \dots, 1000$. The vertical line is the splicing location. Top right: Hill plot (black, solid), together with a mean-of-order -1 bias-reduced estimator (blue, dotted). Bottom left: empirical variance of the LTH as a function of k . Bottom right: slope of a fitted linear model to the LTH as a function of k .

We can immediately see that

$$\mathbb{E}[T_{b,k}] = \xi + \frac{Q_0(n/k)}{p} \frac{\frac{((k+1)/b)^p}{1-p} - 1}{1 + \sum_{j=b+1}^k j^{-1}} (1 + o_p(1)),$$

$$\mathbb{E}[\bar{T}_k] = \xi + \frac{Q_0(n/k)}{pk} \sum_{b=1}^k \frac{\frac{((k+1)/b)^p}{1-p} - 1}{1 + \sum_{j=b+1}^k j^{-1}} (1 + o_p(1)),$$

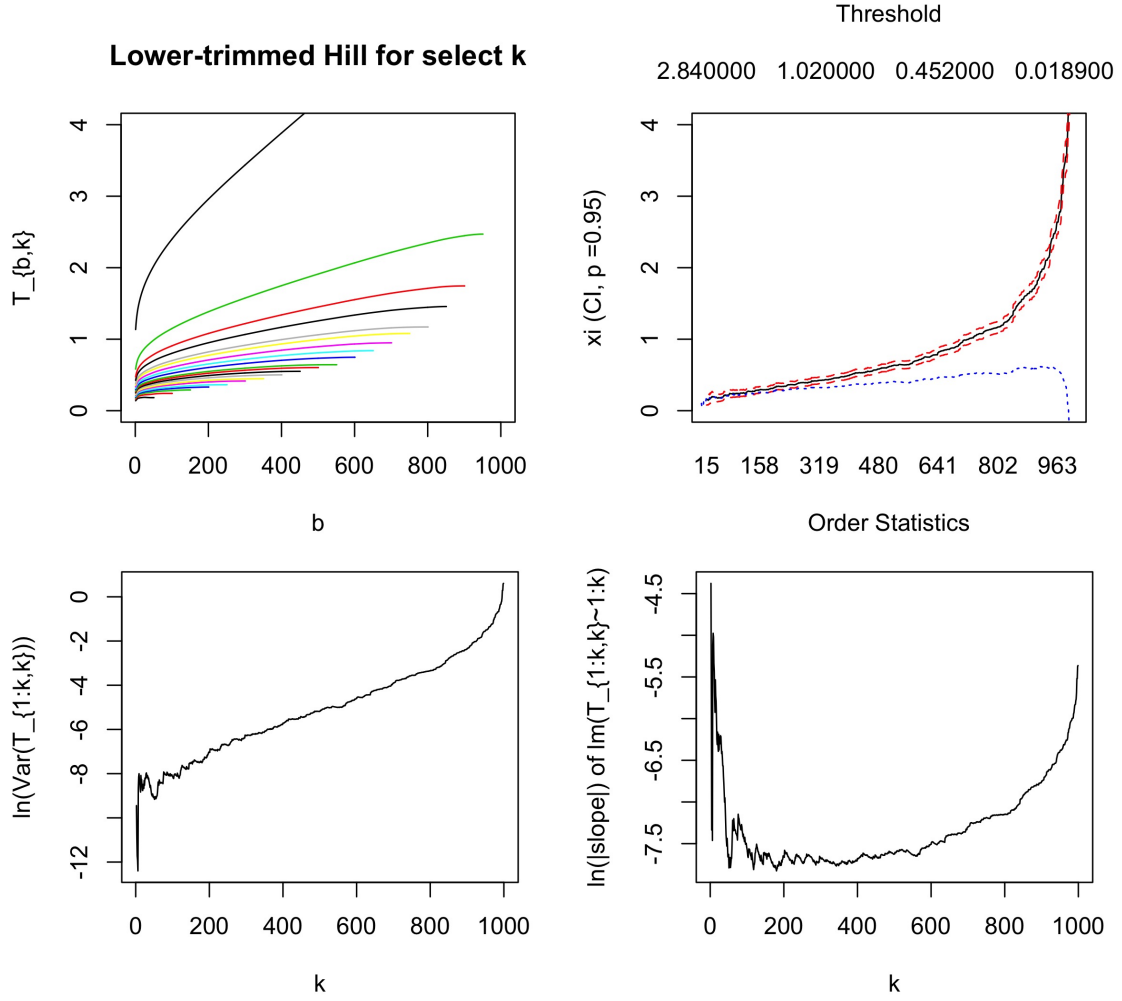


FIGURE 3. Student-t case (10 degrees of freedom). Top left: $T_{b,k}$ for varying lower trimming b , for $k = 1, 51, 101, \dots, 1000$. Top right: Hill plot (black, solid), together with a mean-of-order -1 bias-reduced estimator (blue, dotted). Bottom left: empirical variance of the LTH as a function of k . Bottom right: slope of a fitted linear model to the LTH as a function of k .

so that the asymptotic bias terms can be recognized directly. To ease notation, let us introduce the constants

$$(17) \quad c_{b,k,p} := \frac{1}{p} \cdot \frac{\frac{((k+1)/b)^p - 1}{1-p} - 1}{1 + \sum_{j=b+1}^k j^{-1}} \approx \frac{1}{p} \cdot \frac{\frac{((k+1)/b)^p - 1}{1-p} - 1}{1 + \log((k+1)/b)}$$

$$\bar{c}_{k,p} := \frac{1}{pk} \sum_{b=1}^k \frac{\frac{((k+1)/b)^p - 1}{1-p} - 1}{1 + \sum_{j=b+1}^k j^{-1}} \approx \frac{1}{pk} \sum_{b=1}^k \frac{\frac{((k+1)/b)^p - 1}{1-p} - 1}{1 + \log((k+1)/b)}.$$

Theorem 3.2. *The average \bar{T}_k as defined in (16), under model (1) and second order condition (14) satisfies the following asymptotic distributional identity, for*

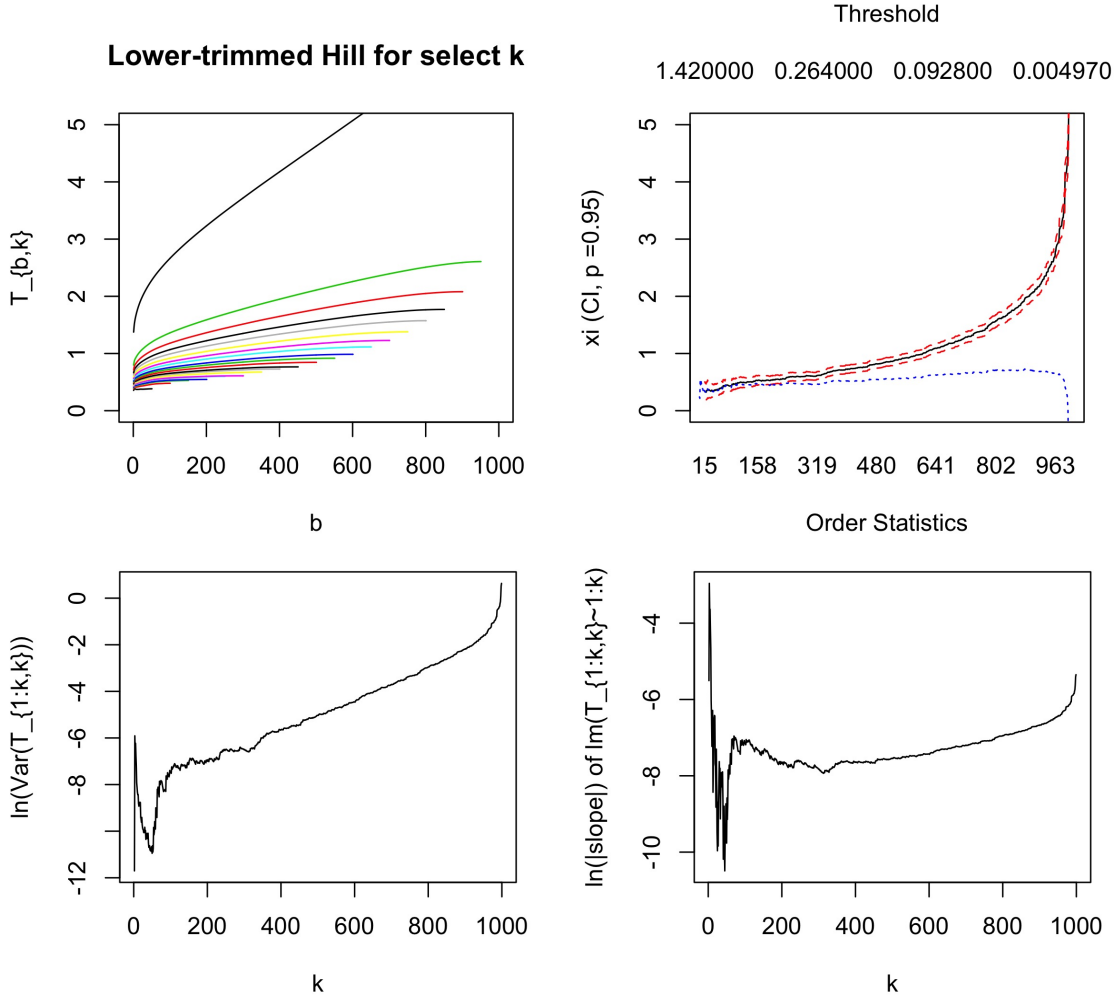


FIGURE 4. Burr case (all parameters set to 1). Top left: $T_{b,k}$ for varying lower trimming b , for $k = 1, 51, 101, \dots, 1000$. Top right: Hill plot (black, solid), together with a mean-of-order -1 bias-reduced estimator (blue, dotted). Bottom left: empirical variance of the LTH as a function of k . Bottom right: slope of a fitted linear model to the LTH as a function of k .

$n, k, n/k \rightarrow \infty$,

$$(18) \quad \bar{T}_k \stackrel{d}{=} \frac{\xi}{k} \sum_{j=1}^k E_j \left[\log(1 + \log(k/j)) + \frac{ek}{j} \mathbf{E}(1 + \log(k/j)) \right] (1 + o(1)) \\ + Q_0(n/k) \left[\frac{e^{1-p}}{p(1-p)} \mathbf{E}(1-p) - \frac{e}{p} \mathbf{E}(1) \right] (1 + o_p(1)),$$

where

$$\mathbf{E}(x) := \int_x^\infty e^{-v}/v \, dv,$$

is the exponential integral.

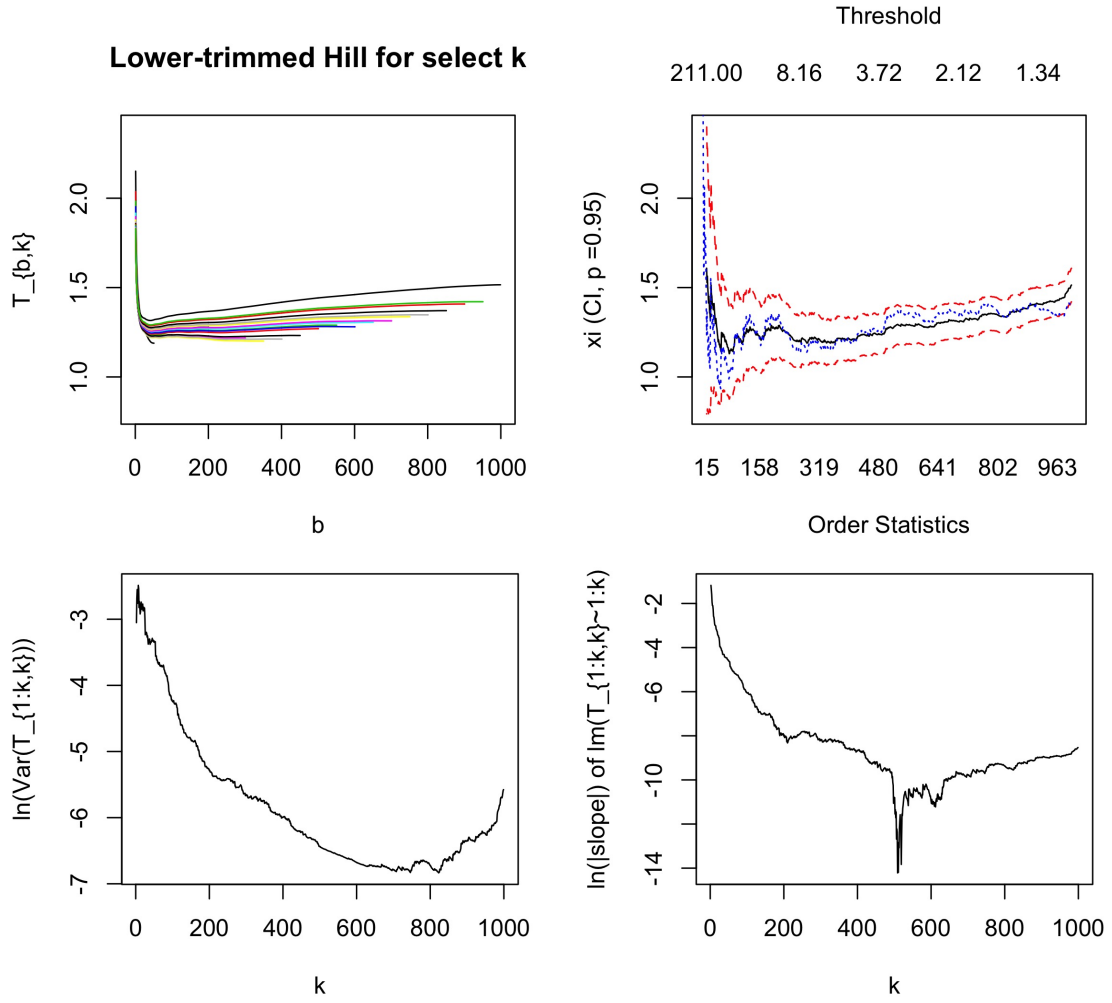


FIGURE 5. Loggamma case (logshape parameter: $3/2$, lograte parameter: 1). Top left: $T_{b,k}$ for varying lower trimming b , for $k = 1, 51, 101, \dots, 1000$. Top right: Hill plot (black, solid), together with a mean-of-order -1 bias-reduced estimator (blue, dotted). Bottom left: empirical variance of the LTH as a function of k . Bottom right: slope of a fitted linear model to the LTH as a function of k .

Equipped with the representations in terms of exponential variables that we obtained in Theorems 3.1 and 3.2, we set on to analyze the mean of the empirical variance of $T_{b,k}$ as a function of b .

Theorem 3.3. *The mean of the empirical variance of $\{T_{b,k}; 1 \leq b \leq k\}$, under model (1) and second order condition (14) satisfies the following asymptotic identity, for $n, k, n/k \rightarrow \infty$,*

$$\mathbb{E} \left[\frac{1}{k} \sum_{b=1}^k (T_{b,k} - \bar{T}_k)^2 \right] = \frac{C}{k} \xi^2(1 + o(1)) + Q_0^2(n/k) f(p)(1 + o_p(1))$$

where $C = 0.502727$ and

$$\begin{aligned}
 f(p) &:= \frac{1 - e^{1-2p}(1-2p)\mathbf{E}(1-2p) - e^{2-2p}\mathbf{E}^2(1-p)}{p^2(1-p)^2} \\
 &+ 2\frac{e^{2-p}\mathbf{E}(1-p)\mathbf{E}(1) - 1 + e^{1-p}(1-p)\mathbf{E}(1-p)}{p^2(1-p)} \\
 (19) \quad &+ \frac{1 - e\mathbf{E}(1) - e^2\mathbf{E}^2(1)}{p^2} > 0.
 \end{aligned}$$

Notice the fact that C and f are universal. A plot of f as a function of p is given in Figure 6.

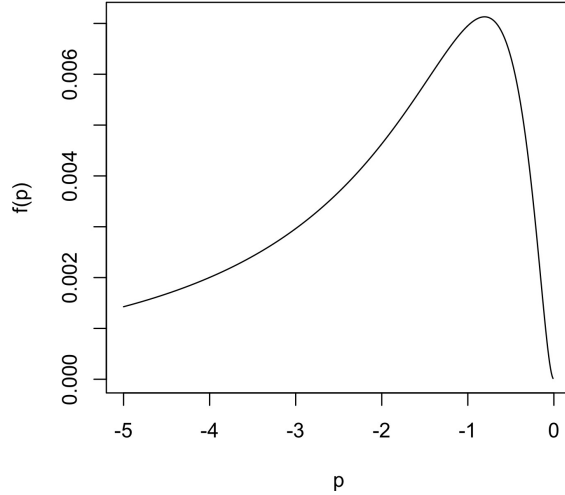


FIGURE 6. Plot of $f(p)$.

3.2. Optimal k in the Hall class. We now make a further assumption on the regularly varying class, in order to get an explicit form of Q_0 . Concretely, we assume the Hall class (Hall (1982)), which satisfies the property

$$(20) \quad U(x) = Ax^\xi(1 + Dx^p(1 + o(1))), \quad x \rightarrow \infty.$$

An immediate consequence then is the explicit expression

$$Q_0(x) = pDx^p(1 + o(1)).$$

Hence,

$$(21) \quad \mathbb{E} \left[\frac{1}{k} \sum_{b=1}^k (T_{b,k} - \bar{T}_k)^2 \right] = \frac{C}{k} \xi^2(1 + o(1)) + Q_0^2\left(\frac{n}{k}\right) f(p)(1 + o_p(1)).$$

Recall that the classical Hill estimator for this class has AMSE given by

$$\frac{\xi^2}{k} + \left(\frac{Q_0(n/k)}{1-p} \right)^2,$$

which is minimized for

$$\begin{aligned} k_0^* &\sim (Q_0^2(n))^{-1/(1-2p)} \left(\frac{\xi^2(1-p)^2}{-2p} \right)^{1/(1-2p)} \\ (22) \quad &= \left(\frac{n^{-2p}\xi^2(1-p)^2}{-2p^3D^2} \right)^{1/(1-2p)}, \end{aligned}$$

see e.g. (Beirlant et al., 2004, p.125)). In a similar way, the minimizer of (21) is simply

$$\begin{aligned} k^* &\sim (Q_0^2(n))^{-1/(1-2p)} \left(\frac{C\xi^2}{-2pf(p)} \right)^{1/(1-2p)} \\ (23) \quad &= \left(\frac{n^{-2p}C\xi^2}{-2p^3D^2f(p)} \right)^{1/(1-2p)}. \end{aligned}$$

Hence from (22) and (23) we obtain a simple expression of the optimal threshold k_0^* of the Hill estimator in terms of k^* :

$$(24) \quad k_0^* = k^* \left(\frac{C}{(1-p)^2f(p)} \right)^{-1/(1-2p)}.$$

3.3. Interpretation of \bar{T}_k as a weighted Hill estimator. Observe that, for fixed k ,

$$(25) \quad \bar{T}_k = \frac{1}{k} \sum_{b=1}^k T_{b,k} = \frac{1}{k} \sum_{i=1}^k \theta_i \log(Y_{i,k}),$$

with

$$\theta_i := \sum_{b=i}^k \frac{1}{b(1 + \sum_{j=b+1}^k j^{-1})},$$

so that one can interpret the estimator \bar{T}_k as a modification of the classical Hill estimator that uses different weights for different order statistics. It is not hard to see that asymptotically the correction factors behave like

$$(26) \quad \theta_i \sim \log \left(\frac{\log(i/k) - 1}{\log(1 - 1/k) - 1} \right), \quad k \rightarrow \infty.$$

Figure 7(left) highlights the accuracy of this approximation for $k = 100$ across different values of i , and also illustrates the fact that the largest data point receives a weight of almost 2 in this case, whereas on from the 20th-largest observation the weight is lower than for the classical Hill estimator, and the weight diminishes for smaller data points. Note that, as k increases, the weight of the largest observation grows above any bound, but extremely slowly, namely

$$\theta_1 = \log(\log(k) + 1) - 1/k + O(1/k^3).$$

Figure 7(right) illustrates that even for a value as large as $k = 10000$, θ_1 is still below 2.4.

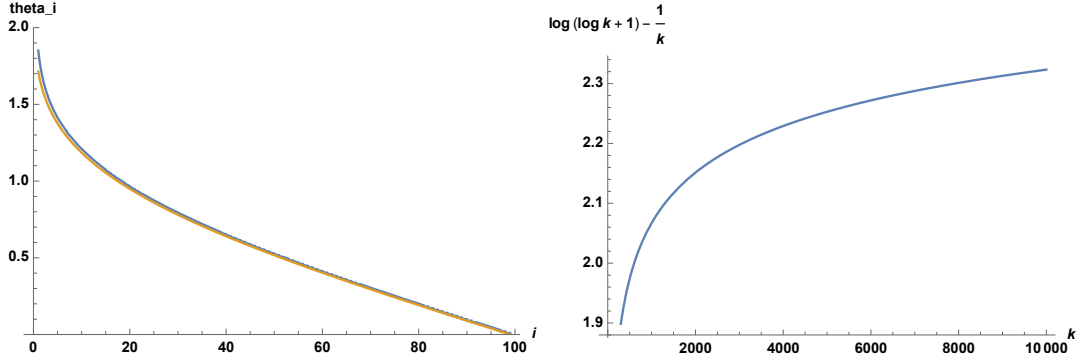


FIGURE 7. Left panel: for $k = 100$, the true θ_i (blue) and the asymptotic approximation from equation (26) (orange) as a function of i . Right panel: Leading terms of the series expansion of θ_1 with respect to k .

4. A RATIO STATISTIC

Once a k^* has been selected, it is important to be able to statistically assess whether the remaining upper tail differs significantly from the one of a pure Pareto. In order to recognize whether a Pareto tail has been achieved or not, we have seen that flatness of the lower-trimmed Hill estimator is desirable. Inspired by the T-statistic introduced in Bhattacharya et al. (2019), we introduce the ratio statistics

$$R_{b,k} = \frac{T_{b+1,k}}{T_{b,k}}, \quad b = 1, \dots, k-1,$$

quantities which we expect to be close to one. Although these statistics do not have the property of being i.i.d. and hence test sizes have to be calibrated using Monte Carlo simulation, an advantage which carries over to the present setting is that they do not depend on ξ . Indeed, defining $\omega(b, k) = b(1 + \sum_{j=b+1}^k j^{-1})$, we have

$$R_{b,k} \stackrel{d}{=} \frac{\omega(b, k)}{\omega(b+1, k)} \left(1 + \frac{\log(\Gamma_{b+1}/\Gamma_{k+1})}{\sum_{i=1}^b \log(\Gamma_i/\Gamma_{k+1})} \right),$$

by the order statistics property of the Poisson process, where, $\Gamma_m = \sum_{i=1}^m E_i$, and E_i , $i = 1, 2, \dots$, is an i.i.d. sequence of independent unit-rate exponential random variables. This invariance with respect to the ξ parameter permits to assess the goodness of selection of a threshold k^* as follows:

- (1) Simulate the R_{b,k^*} statistics N_{MC} times, and call them

$$R_{b,k^*}^m, \quad m = 1, \dots, N_{MC}, \quad b = 2, \dots, k^* - 1.$$

- (2) For fixed $\alpha \in (0, 1)$, find the empirical $\alpha/2$ and $1 - \alpha/2$ quantiles corresponding to each of the $b = 2, \dots, k^* - 1$ samples,

$$R_{b,k^*}^m, \quad m = 1, \dots, N_{MC},$$

and call them $(q_1, q_2)_2, \dots, (q_1, q_2)_{k^*-1}$.

- (3) Count the proportion of the N_{MC} trajectories

$$(R_{b,k^*}^m)_{b=2,\dots,k^*-1},$$

which for *some* $b \in \{2 \dots k^* - 1\}$ fall outside of their confidence interval $(q_1, q_2)_b$. Call this proportion α_r .

- (4) The proportion α_r is the global level of the test, and the algorithm stops when it is close enough to a pre-specified level (typically 0.05). If α_r is larger (smaller) than the pre-specified level, go to Step (2) and decrease (increase) α .
- (5) Plot the R_{b,k^*} , $b = 2, \dots, k^* - 1$, from the data, together with the last set of quantiles $(q_1, q_2)_1, \dots, (q_1, q_2)_{k^*-1}$. It is also a good idea, for visualization, to plot the standardized version

$$\frac{R_{b,k^*} - q_{1,b}}{q_{2,b} - q_{1,b}}, \quad b = 2, \dots, k^* - 1,$$

which for a pure Pareto tail is expected by construction to lie (as a trajectory) between 0 and 1 in $100(1 - \alpha_r)\%$ of the cases. Here, we have used the notation $(q_1, q_2)_b = (q_{1,b}, q_{2,b})$.

Example 4.1. For the Burr sample of Figure 4, we compare taking $k^* = 326$ and $k^* = 600$ in the plots of Figure 8. The first number, $k^* = 326$ is precisely the one that minimizes the expected empirical variance, according to the parameters of the Burr sample and to formula (23), with p chosen to be -1 . The number of Monte Carlo simulations was in each case $N_{MC} = 10000$, and the significance level is $\alpha = 0.05$. Observe how the fit is good for $k = 326$, but is outside the bands for $k = 600$.

Remark 4.1. This approach can only be considered as a selection procedure itself if the corresponding sequential testing is adjusted to have the correct size. In other words, if the above algorithm is used multiple times to choose k , the rejection probability will exceed the desired α level. An alternative is to take sequential values of k into the algorithm, which makes the routine highly computationally intensive. Hence, we presently recommend it solely as a goodness of selection evaluation.

5. SIMULATIONS

We perform a simulation study based on three different and common distributions which belong to the Hall class (20). We consider simulating $N_{sim} = 1000$ times from the following three distributions, with four sub-cases for each distribution, for varying sample size and parameters:

- The Burr distribution, with tail given by

$$\bar{F}(x) = \left(\frac{\eta}{\eta + x^\tau} \right)^\lambda, \quad x > 0, \quad \eta, \tau, \lambda > 0,$$

which implies by Taylor expansion that

$$\xi = \frac{1}{\lambda\tau}, \quad A = \eta^{1/\tau}, \quad D = -\frac{1}{\tau}, \quad p = -\frac{1}{\lambda}.$$

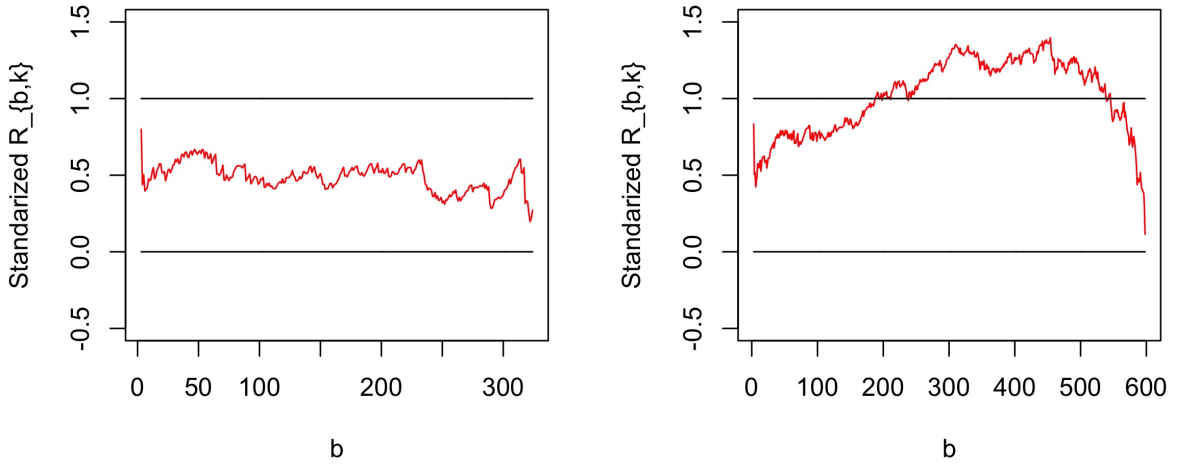


FIGURE 8. Standardized R-statistic for the Burr sample of Figure 4 (all parameters set to 1), for two choices of threshold: $k = 326, 600$, respectively. $N_{MC} = 10000$ and $\alpha = 0.05$.

We consider for $n = 100, 500$ the two sets of parameters $\eta = 1, \lambda = 2, \tau = 1/2$; and $\eta = 3/2, \lambda = 1/2, \tau = 2$.

- The Fréchet distribution with tail

$$\bar{F}(x) = 1 - \exp(-x^{-\alpha}), \quad \alpha > 0,$$

which implies

$$\xi = \frac{1}{\alpha}, \quad A = 1, \quad D = -\frac{1}{2\alpha}, \quad p = -1.$$

We consider for $n = 100, 500$ the two parameters $\alpha = 1, 1/2$.

- The Generalized Pareto Distribution (GPD) distribution, with tail given by

$$\bar{F}(x) = \left(1 + \frac{\gamma x}{\sigma}\right)^{-1/\gamma}, \quad \gamma, \sigma > 0,$$

which implies

$$\xi = \gamma, \quad A = \frac{\sigma}{\gamma}, \quad D = -1, \quad p = -\gamma.$$

We consider for $n = 100, 500$ the two sets of parameters $\gamma = 1/2, \sigma = 2$; and $\gamma = 5/2, \sigma = 1$.

- The Student-t distribution with m degrees of freedom. The tail is given in terms of hypergeometric and Gamma functions. Since this distribution is symmetric around zero, we take the absolute values of the data, which preserves the tail behaviour. We have that

$$\xi = \frac{1}{m}, \quad p = -\frac{2}{m}.$$

We consider, for $n = 100, 500$, the two sets of parameters $m = 2, 10$.

For each sample we evaluate the Hill estimator

$$H_k = T_{k,k}$$

and the averaged trimmed estimator

$$\bar{T}_k = \frac{1}{k} \sum_{b=1}^k T_{b,k}$$

at three particular choices of k . Note that these threshold choices are designed for the Hill estimator, but will turn out sensible for the latter estimator as well.

- (i) We use the popular procedure of Guillou and Hall (2001) as a benchmark for finding the optimal choice of k , and denote the resulting tail estimators by $H_{\hat{k}_{GH}}, \bar{T}_{\hat{k}_{GH}}$. Such a threshold selection procedure has been subject to comparisons (both in Guillou and Hall (2001) itself and in Beirlant et al. (2002)) to other alternatives like Danielsson et al. (2001) and Drees and Kaufmann (1998). We also refer to Schneider et al. (2019) for a recent paper which was developed independently around the same time as the present article.
- (ii) An estimator \hat{k}_0^* of k_0^* from (22) is obtained as follows. Motivated by (21), we compute \hat{k}^* as the minimizer of the empirical variance (the search beginning at $1/5$ of the sample size, to avoid degeneracies) of the trimmed Hill estimator, as a function of b , and using (24) to set

$$\hat{k}_0^* := \hat{k}^* \left(\frac{C}{(1-p)^2 f(p)} \right)^{-1/(1-2p)}.$$

Observe that while we still have to input p , here prior knowledge of ξ, D is no longer needed. We choose $p = -1$ as the canonical choice.

- (iii) As in (ii), but using the true parameter of p , in order to quantify how the removal of a potential misspecification of p by the canonical choice $p = -1$ affects the estimators. The results obtained when using an estimator of p , such as given by Fraga Alves et al. (2003), rather than fixing it at a fixed value, indicated that the additional variability by including an additional estimator does not lead to further improvements at smaller sample sizes. This confirms the observations made for instance in Drees and Kaufmann (1998) and Beirlant et al. (2002).

We then plot the bias, variance and MSE of each resulting estimator as a function of k .

The results are given in Figures 9, 10 for the Burr case; Figures 11, 12 for the Fréchet case; Figures 13, 14 for the GPD case; and Figures 15, 16 for the Student-t case. We observe that the behaviour is very similar for the four families (which is not uncommon in this context, cf. (Beirlant et al., 2002, p.178)).

For the Hill estimator, we notice that our method fares well against the benchmark. The misspecification of the second order parameter p does not play a substantial role, except perhaps for the most biased case of the Student-t distribution with 10 degrees of freedom. The same behaviour is observed within the three \bar{T} -estimators. When comparing Hill against \bar{T} -estimators, the latter improve the bias and MSE for nearly all k , and in most cases also the variance (except for very heavy tails ($\xi \geq 1$) and small values of k).

Remarkably, the estimator $\bar{T}_{k_0, p=-1}$, where the canonical $p = -1$ is used, is highly competitive against the Hill estimator, especially so for $\xi \leq 1$. This is not a contradiction, since the optimality of the Hill estimator refers to choices for k within the class of H_k , whereas the \bar{T}_k estimators span a different class (visible in the weighting interpretation of Section 3.3), and when k is optimized w.r.t. AMSE in that class, even better performance can be feasible, which, however, is not the subject of the present paper.

6. INSURANCE DATA

Let us now consider a real-life insurance data set consisting of 837 motor third party liability (MTPL) insurance claims from the period 1995-2010 that was studied intensively in Albrecher et al. (2017) (where it is referred to as "Company A"). These data are right-censored, and were also analyzed recently combining survival analysis techniques and expert information in Bladt et al. (2019). Here, we focus only on the *ultimates*, see Figure 17, which are the actual final claim sizes for the settled claims and an expert prediction of the total payment until closure for all claims that are still open.

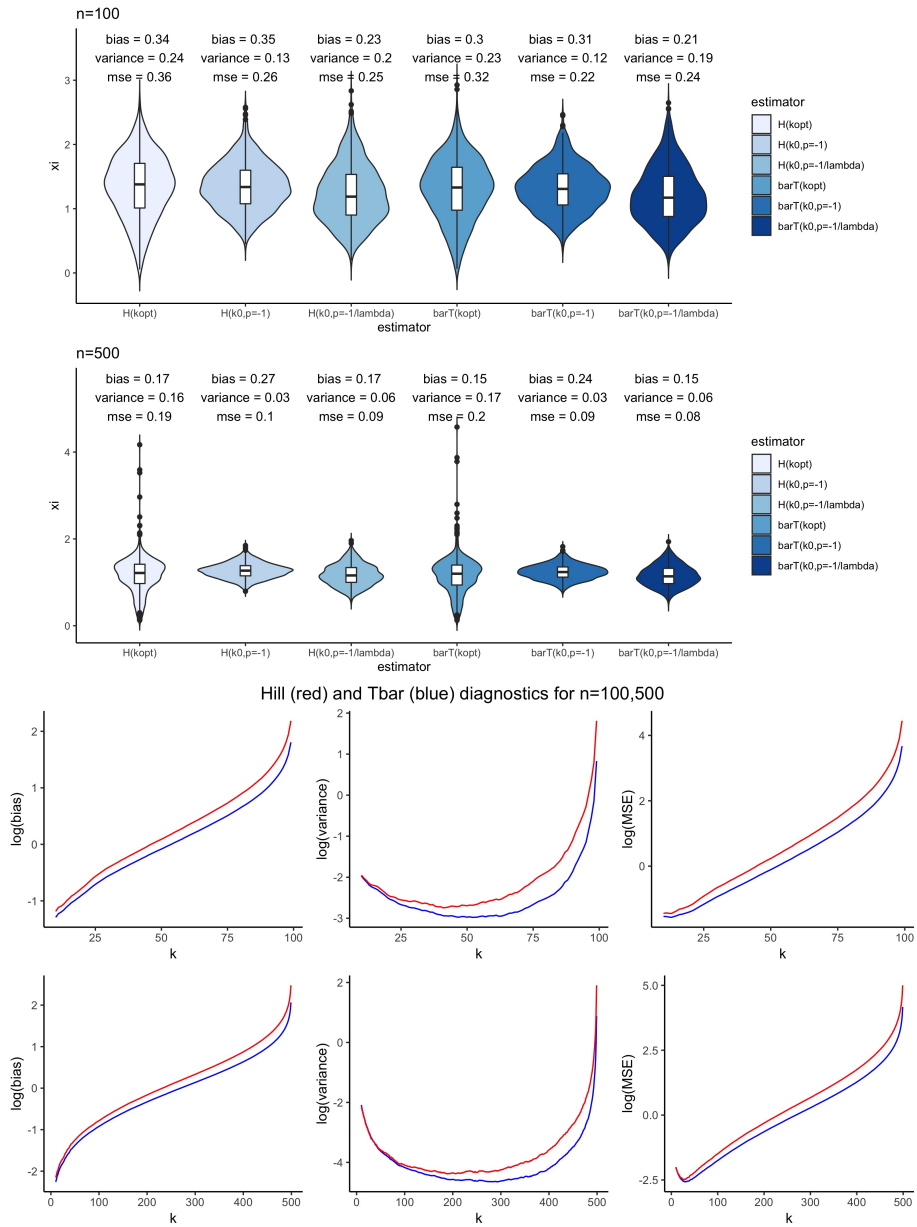


FIGURE 9. Burr distribution, parameters $\eta = 1$, $\lambda = 2$, $\tau = 1/2$. Top: Violin plots for $n = 100, 500$ of the estimators $H_{\hat{k}_{GH}}$, $H_{\hat{k}_0^*, p=-1}$, $H_{\hat{k}_0^*, p=-1/\lambda}$, $\bar{T}_{\hat{k}_{GH}}$, $\bar{T}_{\hat{k}_0^*, p=-1}$, $\bar{T}_{\hat{k}_0^*, p=-1/\lambda}$. Bottom: diagnostics of \bar{T}_k (blue) and H_k (red) as a function of k .

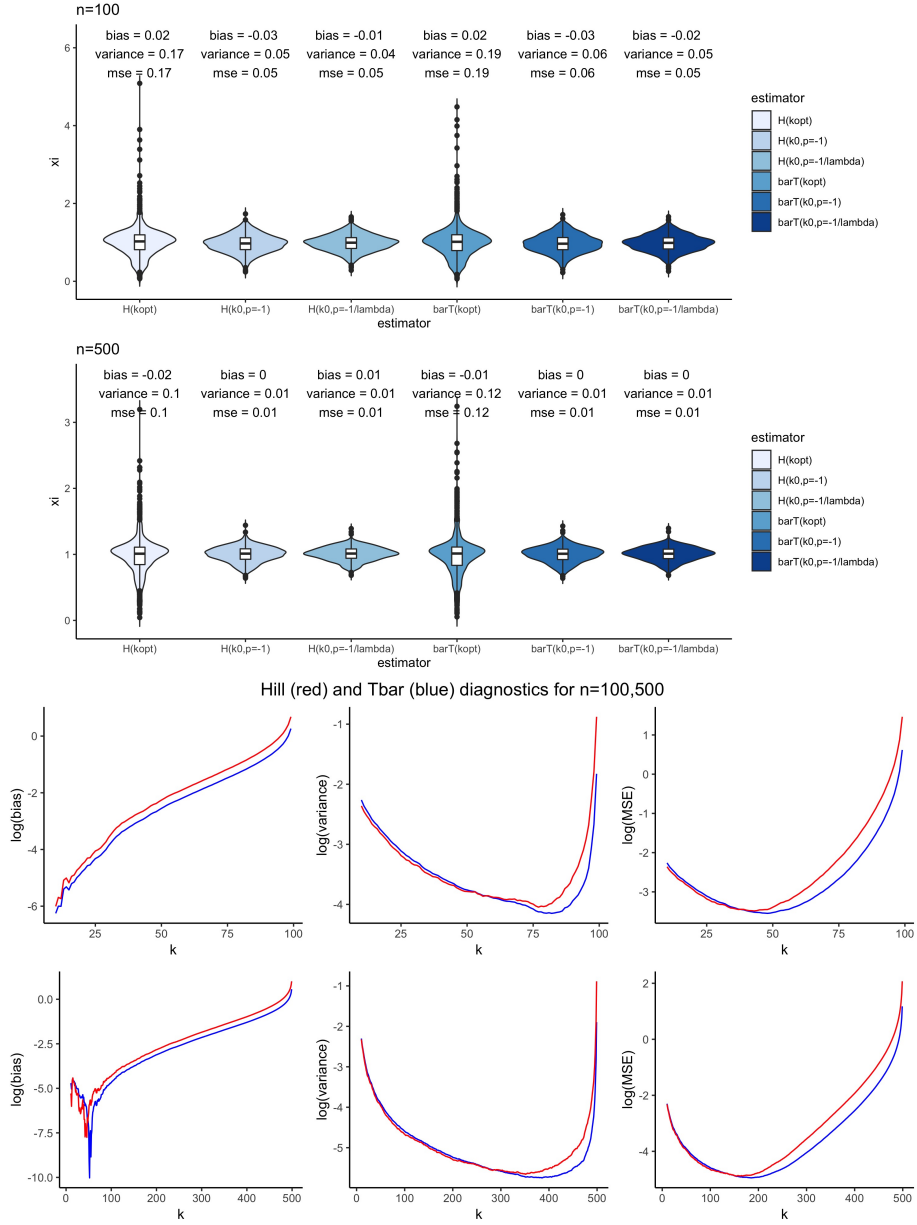


FIGURE 10. Burr distribution, parameters $\eta = 3/2$, $\lambda = 1/2$, $\tau = 2$. Top: Violin plots for $n = 100, 500$ of the estimators $H_{\hat{k}_{GH}}$, $H_{\hat{k}_0^*, p=-1}$, $H_{\hat{k}_0^*, p=-1/\lambda}$, $\bar{T}_{\hat{k}_{GH}}$, $\bar{T}_{\hat{k}_0^*, p=-1}$, $\bar{T}_{\hat{k}_0^*, p=-1/\lambda}$. Bottom: diagnostics of \bar{T}_k (blue) and H_k (red) as a function of k .

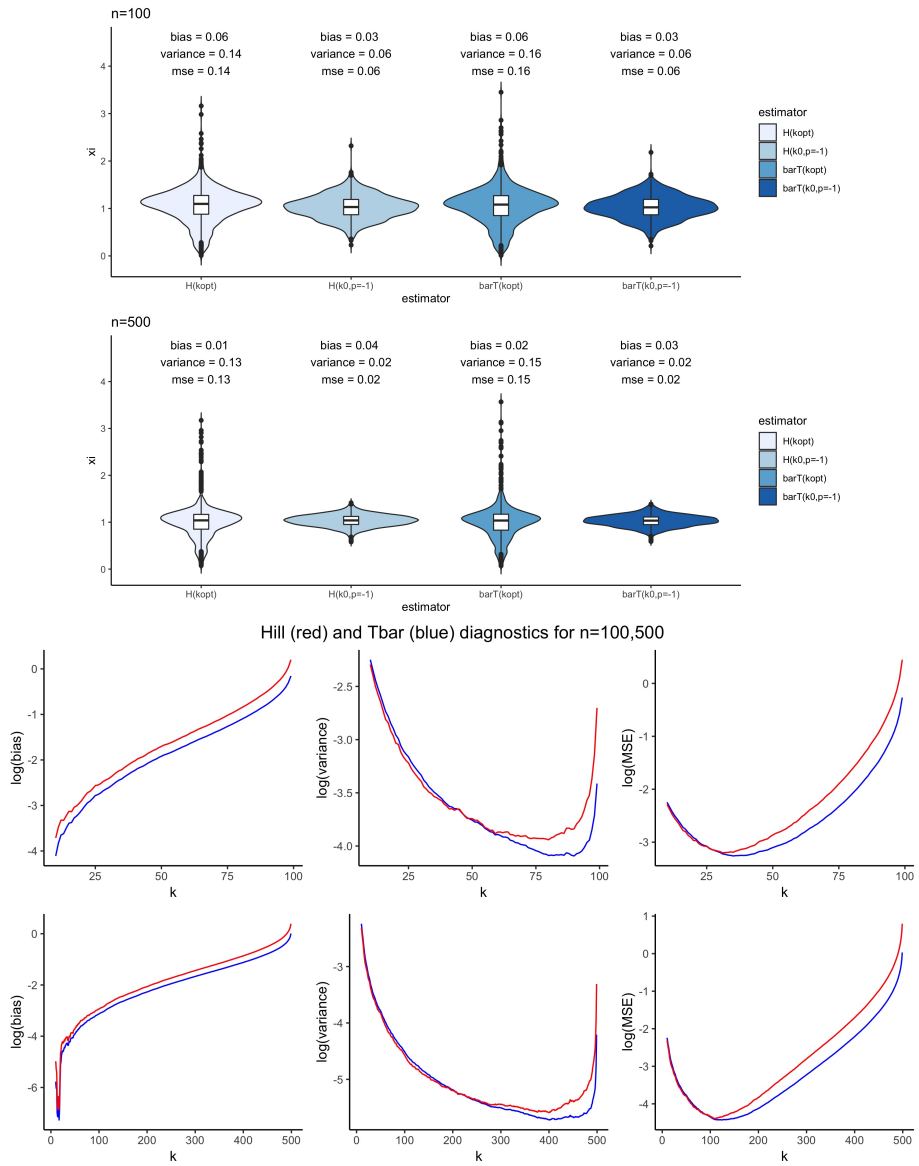


FIGURE 11. Fréchet distribution, parameter $\alpha = 1$. Top: Violin plots for $n = 100, 500$ of the estimators $H_{\hat{k}_{GH}}$, $H_{\hat{k}_0^*, p=-1}$, $\bar{T}_{\hat{k}_{GH}}$, $\bar{T}_{\hat{k}_0^*, p=-1}$. Bottom: diagnostics of \bar{T}_k (blue) and H_k (red) as a function of k .

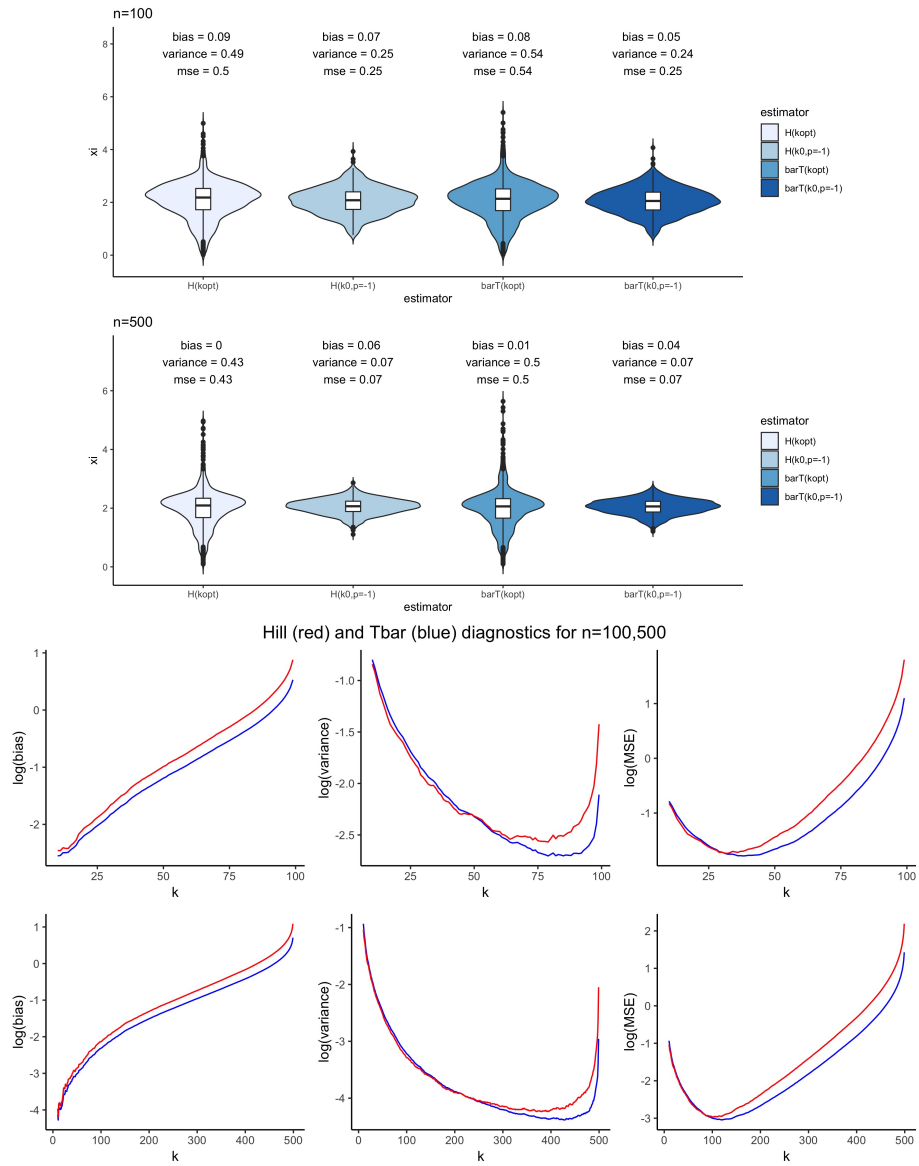


FIGURE 12. Fréchet distribution, parameter $\alpha = 1/2$. Top: Violin plots for $n = 100, 500$ of the estimators $H_{\hat{k}_{GH}}$, $H_{\hat{k}_0^*, p=-1}$, $\bar{T}_{\hat{k}_{GH}}$, $\bar{T}_{\hat{k}_0^*, p=-1}$. Bottom: diagnostics of \bar{T}_k (blue) and H_k (red) as a function of k .

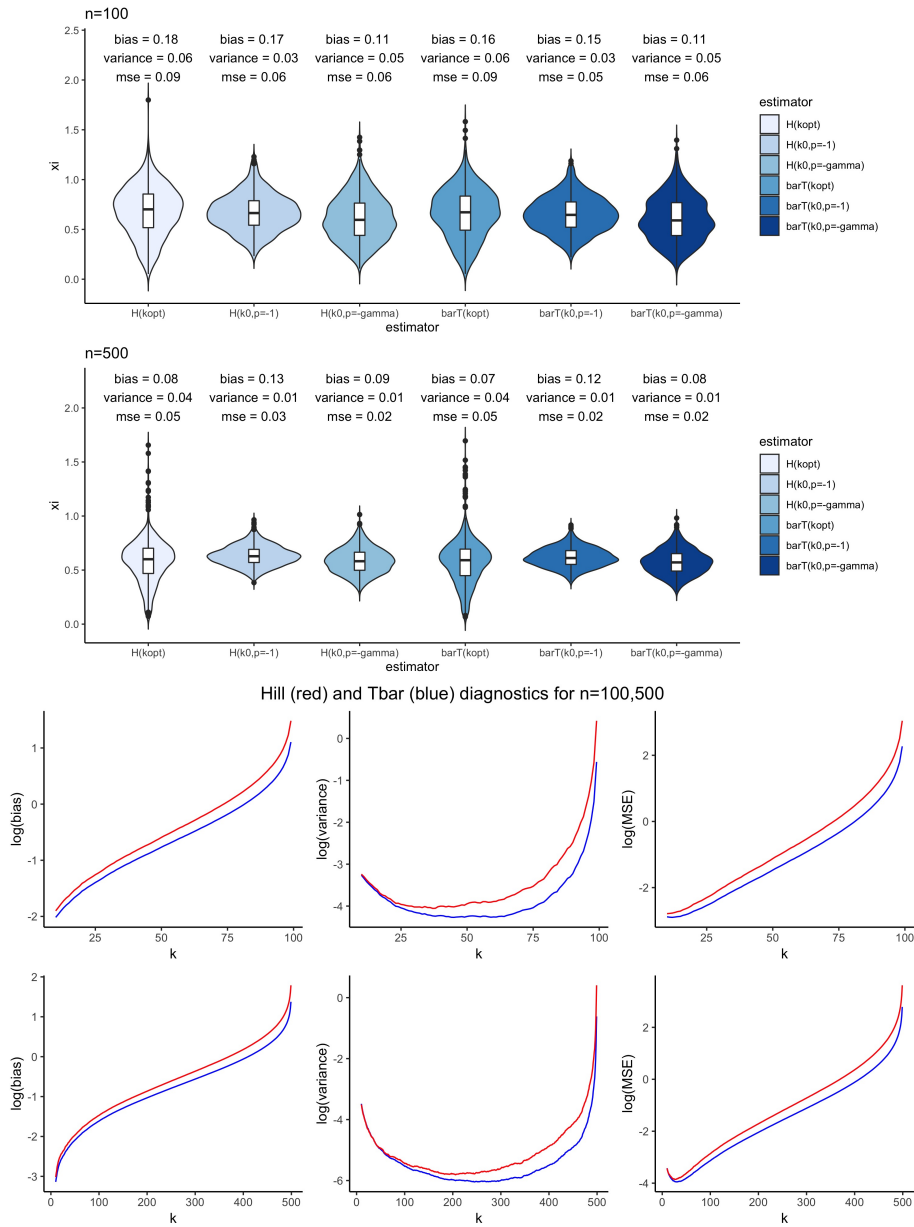


FIGURE 13. GPD distribution, parameters $\gamma = 1/2$, $\sigma = 2$. Top: Violin plots for $n = 100, 500$ of the estimators $H_{\hat{k}_{GH}}$, $H_{\hat{k}_0^*, p=-1}$, $H_{\hat{k}_0^*, p=-\gamma}$, $\bar{T}_{\hat{k}_{GH}}$, $\bar{T}_{\hat{k}_0^*, p=-1}$, $\bar{T}_{\hat{k}_0^*, p=-\gamma}$. Bottom: diagnostics of \bar{T}_k (blue) and H_k (red) as a function of k .

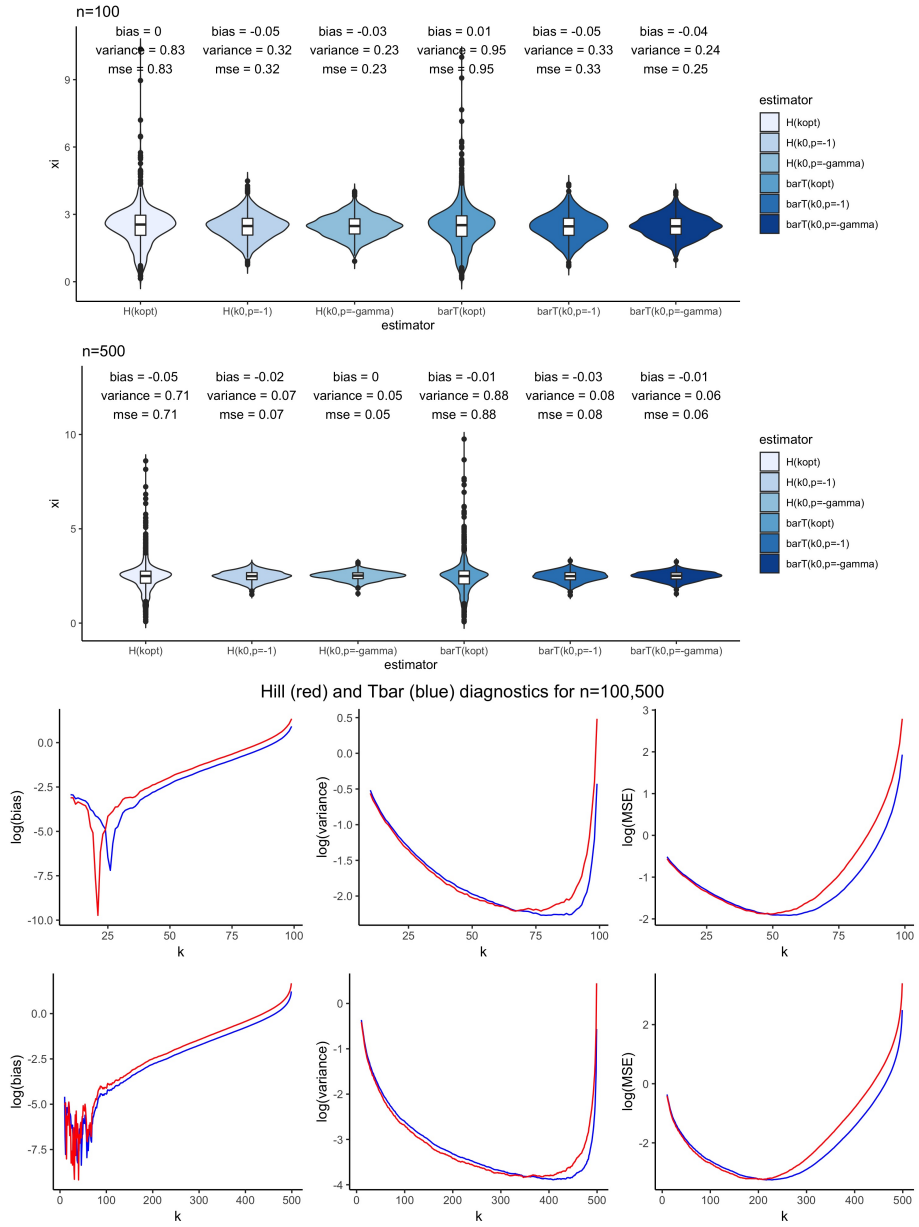


FIGURE 14. GPD distribution, parameters $\gamma = 5/2$, $\sigma = 1$. Top: Violin plots for $n = 100, 500$ of the estimators $H_{\hat{k}_{GH}}$, $H_{\hat{k}_0^*, p=-1}$, $H_{\hat{k}_0^*, p=-\gamma}$, $\bar{T}_{\hat{k}_{GH}}$, $\bar{T}_{\hat{k}_0^*, p=-1}$, $\bar{T}_{\hat{k}_0^*, p=-\gamma}$. Bottom: diagnostics of \bar{T}_k (blue) and H_k (red) as a function of k .

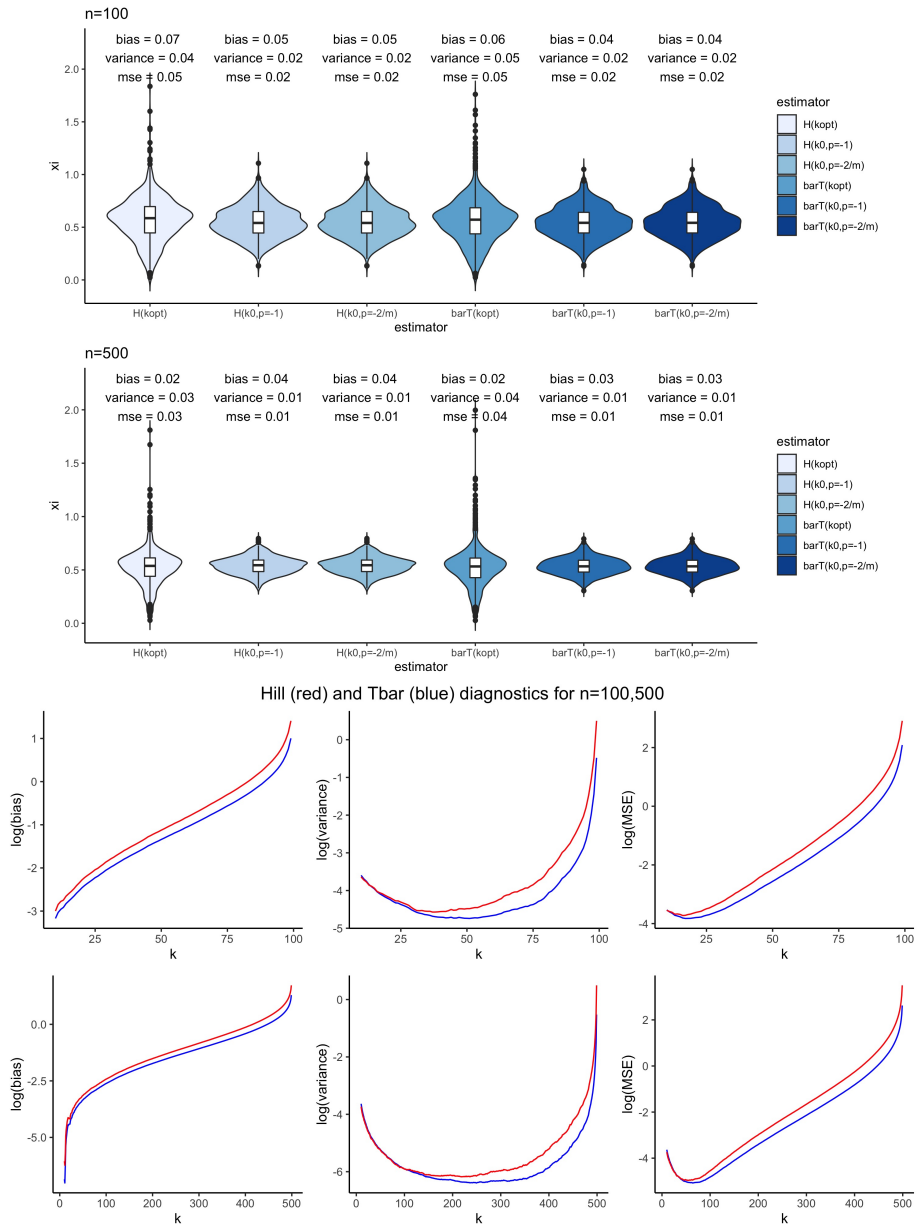


FIGURE 15. Student-t distribution, degrees of freedom $m = 2$. Top: Violin plots for $n = 100, 500$ of the estimators $H_{\hat{k}_{GH}}$, $H_{\hat{k}_0^*, p=-1}$, $H_{\hat{k}_0^*, p=-2/m}$, $\bar{T}_{\hat{k}_{GH}}$, $\bar{T}_{\hat{k}_0^*, p=-1}$, $\bar{T}_{\hat{k}_0^*, p=-2/m}$. Bottom: diagnostics of \bar{T}_k (blue) and H_k (red) as a function of k .

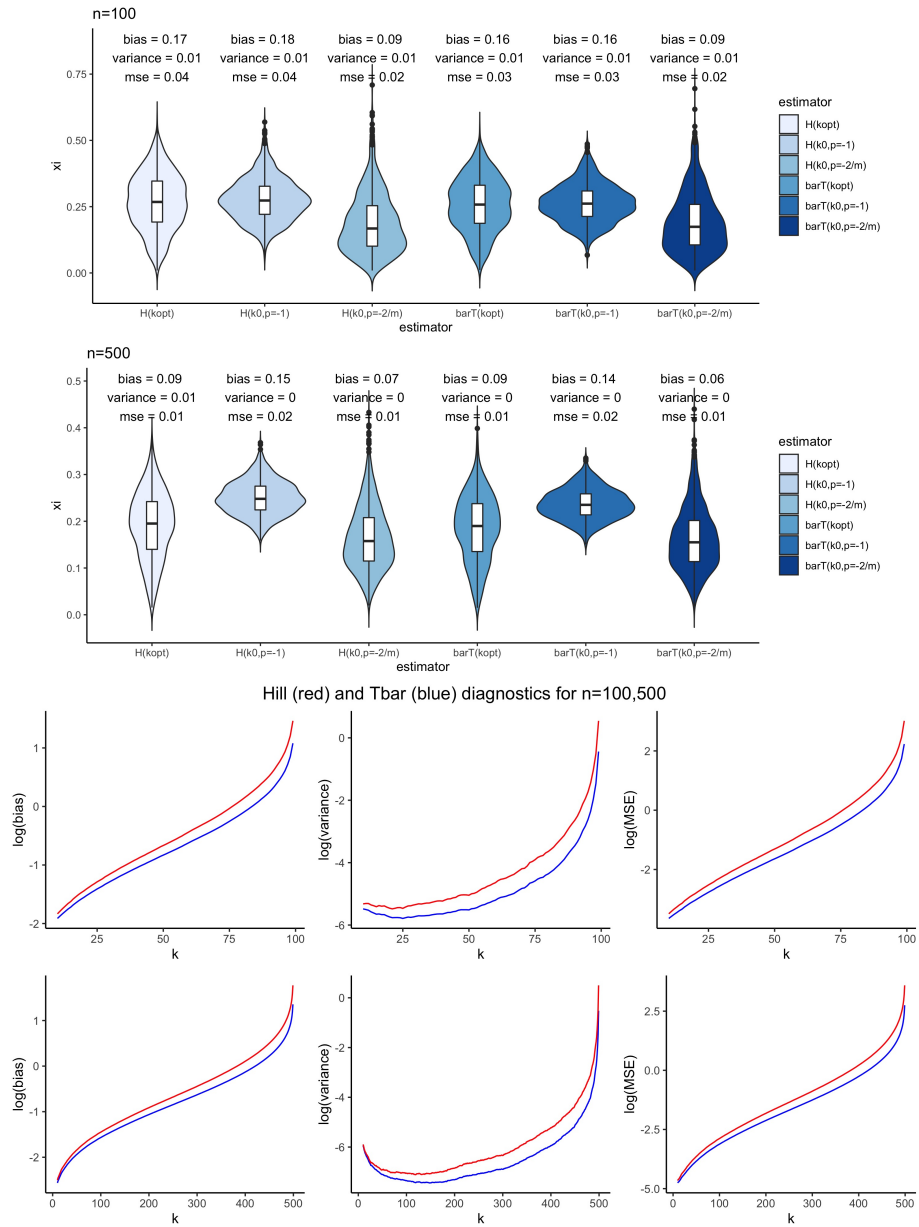


FIGURE 16. Student-t distribution, degrees of freedom $m = 10$. Top: Violin plots for $n = 100, 500$ of the estimators $H_{\hat{k}_{GH}}$, $H_{\hat{k}_0^*, p=-1}$, $H_{\hat{k}_0^*, p=-2/m}$, $\bar{T}_{\hat{k}_{GH}}$, $\bar{T}_{\hat{k}_0^*, p=-1}$, $\bar{T}_{\hat{k}_0^*, p=-2/m}$. Bottom: diagnostics of \bar{T}_k (blue) and H_k (red) as a function of k .

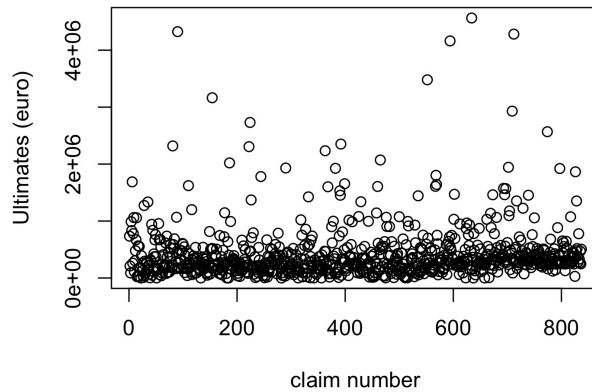


FIGURE 17. Ultimates from an MTPL insurance portfolio.

In Figure 18 we depict the lower-trimmed Hill plots and the usual Hill plot, together with the empirical variance. We have also included \bar{T}_k , which follows somewhat closely the trajectory of the usual Hill plot, and the mean-of-order -1 bias-reduced estimator. As a preliminary observation, notice that the k -area at which visually the Hill plot and its bias-reduced version start to differ is roughly the same as where the lower trimmed Hill trajectories start flattening out, which serves as a good sanity check. As in the simulation studies in Section 5, in order to avoid degeneracies, we only look at candidates for the minimizer to the right of $n/5$, which corresponds to 167 in this case. The minimum empirical variance is then obtained for $\hat{k}^* = 222$. Using the canonical choice $p = -1$, we have that $\hat{k}_0^* = 222/2.62421 \approx 85$. Note that for the same choice $p = -1$, using the prior eyeballed estimate $\xi \approx 0.5$, and based on the Burr-like Hill plot, we can deduce that $\lambda = -1/p = 1$, and then $D = 1/\tau = -\xi = -0.5$. We thus get by (22) the ad-hoc sample fraction $k^{ah} = 112$ (which might be considered the classical choice of the threshold in this case). Notice, however, that the latter estimate is only available heuristically, since one needs a first estimate of ξ to estimate ξ itself, and also to make distributional assumptions on the data. We include this estimate here simply as a naive solution that requires no further statistical procedures beyond looking at the Hill plot.

The corresponding estimates of ξ are given by

$$H_{\hat{k}_0^*} = 0.508, \quad H_{k^{ah}} = 0.560, \quad \bar{T}_{\hat{k}_0^*} = 0.480, \quad \bar{T}_{k^{ah}} = 0.525.$$

The simulation studies of Section 5 may suggest the third of the above numbers to be the most reliable estimate, since there is no way of quantifying the eyeball-aided procedure involving k^{ah} . However, the 95% confidence interval for the first estimate is (0.400, 0.616), suggesting that for a one-sample analysis, it is difficult to make a definitive statement on the statistical superiority of any of the four estimates. Further, the ratio statistic test in Figure 19 suggests that for both thresholds the sample is Pareto in the tail (with only a slight issue for the two largest observations). The takeaway is that, roughly speaking, we are able to reconfirm in an automated statistical way what can be deduced by looking at a Hill plot (together with its bias-reduced variants) and guessing the distribution of the sample.

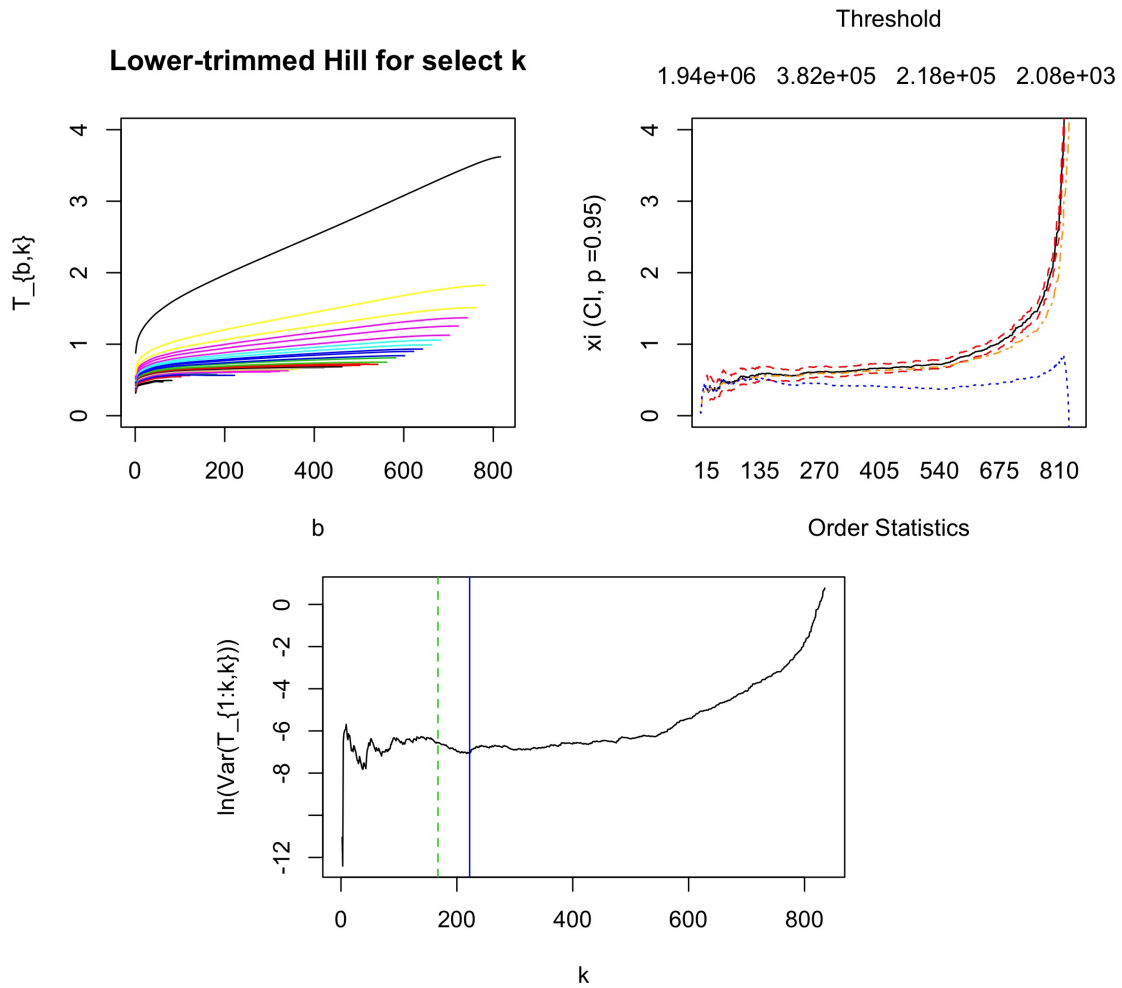


FIGURE 18. MTPL insurance ultimates. Top left: Lower-trimmed Hill estimator (LTH) estimator for varying lower trimming b , for k uniformly spaced from 1 to 837 in units of 20. Top right: Hill plot (black, solid), together with \bar{T}_k (orange, dashed-and-dotted) and a mean-of-order -1 bias-reduced estimator (blue, dotted). Bottom: empirical variance of the LTH as a function of k . The dotted line is the left limit for candidates, and the solid line is the resulting minimum.

In (Albrecher et al., 2017, p.99), a splicing point was suggested for this data set at around $k = 20$, based on expert opinion. A semi-automated option using our method for detecting this splicing point would be to replace the left limit $k = 167$ by a very small number (in this case $k = 4$ is chosen after visual inspection of the erratic nature of the empirical variance for the first three), and then to apply our method, which leads to the detection of the minimum variance at $k = 38$ (which is clearly visible in Figure 18). Under the assumption $p = -1$ this then leads to $k \approx 14$ as a suggested splicing point. We would like to point out that the identification of the splicing point matters in insurance practice, since the different resulting distributional assumptions on either side then have an effect on the location of extreme quantiles and risk management in general, including

the capital requirements for solvency purposes. The possibly natural existence of splicing points can also be argued from a causal perspective, as different degrees of inspection scrutiny may be applied below and above certain claim levels.

As a side remark, in the present data set the ultimates for the highest claims have a certain degree of intrinsic uncertainty (as they are just estimates of the final closed claim size), and a more systematic way to approach this particular situation would be to combine the trimming of the Hill estimator from below and above, but the latter is not the focus of the present paper.

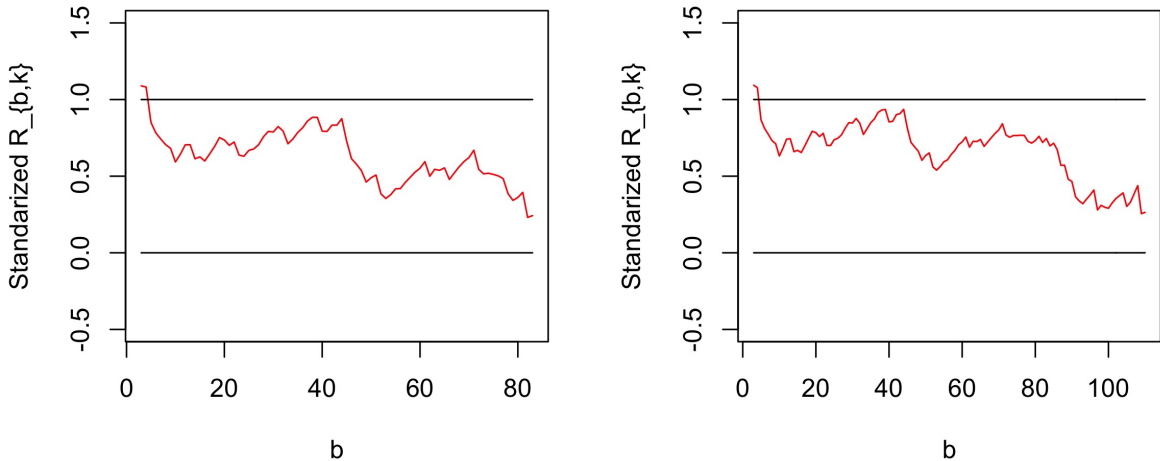


FIGURE 19. Standardized R-statistic for the MTPL ultimates, for the two threshold choices $k = 85$ (left) and $k = 112$ (right). $N_{MC} = 100,000$ and $\alpha = 0.05$.

7. CONCLUSION

In this paper, we showed that trimming the Hill estimator from the left can lead to favorable properties in connection with the expected empirical variance of the tail index estimators in extreme value statistics. For the Hall class, we established asymptotic results on the behavior of this expected empirical variance, which allows to develop a guideline for the choice of the optimal threshold in the tail index estimation problem. It turns out that there is an intrinsic link between this optimal threshold and the classical optimal threshold for the Hill estimator. Since in the trimming context the identification of the optimal threshold is much more insensitive on the tail characteristics (it only depends on the p -parameter in the Hall class, not on D nor on the tail index ξ), this link allows to circumvent the classical problem in threshold selection for the Hill estimator. As a by-product, by suitable averaging we develop a novel tail index estimator which assigns a non-uniform weight to each observation in a natural way, relies on fewer assumptions on the tail characteristics, is simple to implement and outperforms the classical Hill estimator in most cases. The latter is illustrated in simulation studies. In addition, the technique is applied to a real-life insurance data set that was previously studied by other techniques. Note also that the proposed selection principle for k based on the variance of the lower-trimmed Hill plots can be applied to any estimator of ξ for which the asymptotic mean squared

error can be written as $M_1\xi^2/k + M_2(p)Q_0(n/k)^2$ with $M_1 > 0$ and $M_2(p) > 0$ only depending on p . We conclude by noting that the approach taken in this paper is in principle also applicable for the potential improvement of tail index estimators other than the Hill estimator. Further possible directions of future research include the combination of left trimming with right trimming in situations with possible outliers, as well as the consideration of possibly censored data.

Acknowledgement. M.B. and H.A. acknowledge financial support from the Swiss National Science Foundation Project 200021_191984.

REFERENCES

- Albrecher, H., Beirlant, J., and Teugels, J. L. (2017). *Reinsurance: Actuarial and Statistical Aspects*. John Wiley & Sons, Chichester.
- Bader, B., Yan, J., and Zhang, X. (2018). Automated threshold selection for extreme value analysis via ordered goodness-of-fit tests with adjustment for false recovery rate. *Ann. Appl. Statistics*, 12:310–329.
- Beirlant, J., Boniphace, E., and Dierckx, G. (2011). Generalized sum plots. *REVSTAT-Statistical Journal*, 9(2):181–198.
- Beirlant, J., Dierckx, G., Guillou, A., and Stărică, C. (2002). On exponential representations of log-spacings of extreme order statistics. *Extremes*, 5(2):157–180.
- Beirlant, J., Goegebeur, Y., Segers, J., and Teugels, J. L. (2004). *Statistics of extremes: theory and applications*. John Wiley & Sons, Chichester.
- Beirlant, J., Vynckier, P., and Teugels, J. L. (1996). Tail index estimation, pareto quantile plots regression diagnostics. *Journal of the American Statistical Association*, 91(436):1659–1667.
- Bhattacharya, S., Kallitsis, M., and Stoev, S. (2019). Data-adaptive trimming of the Hill estimator and detection of outliers in the extremes of heavy-tailed data. *Electronic Journal of Statistics*, 13:1872–1925.
- Bladt, M., Albrecher, H., and Beirlant, J. (2019). Combined tail estimation using censored data and expert information. *Scandinavian Actuarial Journal*, DOI:10.1080/03461238.2019.1694974.
- Buitendag, S., Beirlant, J., and de Wet, T. (2019). Ridge regression estimators for the extreme value index. *Extremes*, 22:271–292.
- Csörgő, S., Deheuvels, P., and Mason, D. (1985). Kernel estimates of the tail index of a distribution. *Ann. Statist.*, 13(3):1050–1077.
- Danielsson, J., de Haan, L., Peng, L., and de Vries, C. G. (2001). Using a bootstrap method to choose the sample fraction in tail index estimation. *Journal of Multivariate analysis*, 76(2):226–248.
- de Haan, L. and Ferreira, A. (2007). *Extreme value theory: an introduction*. Springer Science & Business Media.
- De Sousa, B. and Michailidis, G. (2004). A diagnostic plot for estimating the tail index of a distribution. *Journal of Computational and Graphical Statistics*, 13(4):974–995.
- Draisma, G., de Haan, L., Peng, L., and Pereira, T. T. (1999). A bootstrap-based method to achieve optimality in estimating the extreme-value index. *Extremes*, 2(4):367–404.

- Drees, H., de Haan, L., and Resnick, S. (2000). How to make a Hill plot. *The Annals of Statistics*, 28(1):254–274.
- Drees, H., Janßen, A., Resnick, S. I., and Wang, T. (2020). On a minimum distance procedure for threshold selection in tail analysis. *SIAM Journal on Mathematics of Data Science*, 2(1):75–102.
- Drees, H. and Kaufmann, E. (1998). Selecting the optimal sample fraction in univariate extreme value estimation. *Stochastic Processes and their Applications*, 75(2):149–172.
- Embrechts, P., Klüppelberg, C., and Mikosch, T. (2013). *Modelling extremal events: for insurance and finance*, volume 33. Springer Science & Business Media, second edition.
- Fraga Alves, M., Gomes, M., and de Haan, L. (2003). A new class of semi-parametric estimators of the second order parameter. *Portugaliae Mathematica*, 60:193–213.
- Gomes, M. I., Brillhante, M. F., and Pestana, D. (2016). New reduced-bias estimators of a positive extreme value index. *Communications in Statistics - Simulation and Computation*, 45(3):833–862.
- Gomes, M. I., de Haan, L., and Rodrigues, L. H. (2008). Tail index estimation for heavy-tailed models: accommodation of bias in weighted log-excesses. *Journal of the Royal Statistical Society: Series B (Statistical Methodology)*, 70(1):31–52.
- Gomes, M. I. and Guillou, A. (2015). Extreme value theory and statistics of univariate extremes: a review. *International Statistical Review*, 83(2):263–292.
- Gomes, M. I. and Oliveira, O. (2001). The bootstrap methodology in statistics of extremes: choice of the optimal sample fraction. *Extremes*, 4(4):331–358.
- Gomes, M. I. and Pestana, D. (2007). A sturdy reduced-bias extreme quantile (var) estimator. *Journal of the American Statistical Association*, 102(477):280–292.
- Guillou, A. and Hall, P. (2001). A diagnostic for selecting the threshold in extreme value analysis. *Journal of the Royal Statistical Society: Series B (Statistical Methodology)*, 63(2):293–305.
- Hall, P. (1982). On some simple estimates of an exponent of regular variation. *J. Roy. Statist. Soc. Ser. B*, 44(1):37–42.
- Hall, P. (1990). Using the bootstrap to estimate mean squared error and select smoothing parameter in nonparametric problems. *Journal of multivariate analysis*, 32(2):177–203.
- Hall, P., Welsh, A., et al. (1985). Adaptive estimates of parameters of regular variation. *The Annals of Statistics*, 13(1):331–341.
- Hill, B. M. (1975). A simple general approach to inference about the tail of a distribution. *The Annals of Statistics*, 3:1163–1174.
- Papastathopoulos, I. and Tawn, J. (2013). Extended generalised pareto models for tail estimation. *Journal of Statistical Planning and Inference*, 143(1):131–143.
- Schneider, L., Krajina, A., and Krivobokova, T. (2019). Threshold selection in univariate extreme value analysis. *Arxiv:1903.02517v1*.

8. PROOFS

Proof of Proposition 2.1. Set $q = k - b + 1$. By the Rényi representation (6),

$$\mathbb{V}[T_{b,k}] = \mathbb{V}\left[\sum_{j=1}^k E_j^* \sum_{i=j \vee q}^k \frac{\gamma_i}{k-j+1}\right] = \xi^2 \frac{\sum_{j=1}^k \left(\frac{k-j \vee q + 1}{k-j+1}\right)^2}{\left(\sum_{j=1}^k \frac{k-j \vee q + 1}{k-j+1}\right)^2}.$$

Plugging in $q = 1$ ($b = k$) gives

$$\mathbb{V}[T_{k,k}] = \frac{\xi^2}{k},$$

which corresponds to the usual variance of the Hill estimator $T_{k,k}$ and gives the first identity. In the general case,

$$\mathbb{V}[T_{b,k}] = \xi^2 \frac{\sum_{j=1}^q \left(\frac{k-q+1}{k-j+1}\right)^2 + k - q + 1}{\left(\sum_{j=1}^q \frac{k-q+1}{k-j+1} + k - q + 1\right)^2}.$$

But $j \leq q$ implies $\frac{k-q+1}{k-j+1} \leq 1$, such that

$$\sum_{j=1}^q \frac{1}{k-j+1} \geq \sum_{j=1}^q \frac{k-q+1}{k-j+1} \frac{1}{k-j+1},$$

so

$$\sum_{j=1}^q \frac{k-q+1}{k-j+1} + k - q + 1 \geq \sum_{j=1}^q \left(\frac{k-q+1}{k-j+1}\right)^2 + k - q + 1.$$

Thus

$$\begin{aligned} \mathbb{V}[T_{b,k}] &\leq \xi^2 \frac{\sum_{j=1}^q \left(\frac{k-q+1}{k-j+1}\right)^2 + k - q + 1}{\left(\sum_{j=1}^q \left(\frac{k-q+1}{k-j+1}\right)^2 + k - q + 1\right)^2} \\ &= \frac{\xi^2}{\sum_{j=1}^q \left(\frac{k-q+1}{k-j+1}\right)^2 + k - q + 1}, \end{aligned}$$

which gives the second identity. \square

Proof of Theorem 3.1. We first note that

$$T_{b,k} \stackrel{d}{=} \frac{\sum_{i=1}^b \log(U(Y_{n-i+1,n})/U(Y_{n-k,n}))}{b(1 + \sum_{j=b+1}^k j^{-1})},$$

where $Y_{1,n} < \dots < Y_{n,n}$ are the order statistics of a standard Pareto sample (the $\xi = 1$ case). Then, from the second order condition (14) we obtain that for $A = Y_{n-k,n}$ and $x = Y_{n-i+1,n}/Y_{n-k,n}$, as $k, n, n/k \rightarrow \infty$,

$$T_{b,k} \stackrel{d}{=} \frac{\xi \sum_{i=1}^b \log(Y_{n-i+1,n}/Y_{n-k,n}) + \frac{Q_0(Y_{n-k,n})}{p} \sum_{i=1}^b ((Y_{n-i+1,n}/Y_{n-k,n})^p - 1)(1 + o_p(1))}{b(1 + \sum_{j=b+1}^k j^{-1})}.$$

But by the Rényi representation (6) of exponential order statistics, the first term is distributed as

$$\sum_{i=1}^b \log(Y_{n-i+1,n}/Y_{n-k,n}) \stackrel{d}{=} \sum_{j=1}^b E_j + b \sum_{j=b+1}^k E_j/j,$$

where E_1, E_2, \dots, E_k are i.i.d. standard exponential random variables. For the second term, by convergence to uniform random variables and a Riemann integral approximation, we get

$$\begin{aligned} \frac{1}{b} \sum_{i=1}^b ((Y_{n-i+1,n}/Y_{n-k,n})^p - 1) &\approx \frac{1}{b} \sum_{i=1}^b (((k+1)/i)^p - 1) \\ &\approx \frac{k+1}{b} \int_0^{b/(k+1)} (u^{-p} - 1) du = \frac{((k+1)/b)^p}{1-p} - 1, \end{aligned}$$

and since $(1 - 1/Y_{n-k,n})$ is a uniform order statistic, we further get that

$$\frac{Q_0(Y_{n-k,n})}{Q_0(n/k)} \xrightarrow{P} 1.$$

Putting the three pieces together then establishes (15). \square

Proof of Theorem 3.2. With the shortened notation, we write

$$(27) \quad T_{b,k} \stackrel{d}{=} \xi \frac{\bar{E}_b + \sum_{j=b+1}^k E_j/j}{1 + \sum_{j=b+1}^k j^{-1}} + Q_0(n/k) c_{b,k,p}(1 + o_p(1)),$$

and by exchange of the order of summation, we can write

$$\begin{aligned} \bar{T}_k &\stackrel{d}{=} \frac{\xi}{k} \sum_{b=1}^k \frac{\bar{E}_b + \sum_{j=b+1}^k E_j/j}{1 + \sum_{j=b+1}^k j^{-1}} + Q_0(n/k) \bar{c}_{k,p}(1 + o_p(1)) \\ &= \frac{\xi}{k} \left[\sum_{j=1}^k E_j \sum_{b=j}^k \frac{1}{b(1 + \sum_{j=b+1}^k j^{-1})} + \sum_{j=2}^k E_j \sum_{b=1}^{j-1} \frac{1}{j(1 + \sum_{j=b+1}^k j^{-1})} \right] \\ &\quad + Q_0(n/k) \bar{c}_{k,p}(1 + o_p(1)) \\ &= \frac{\xi}{k} \sum_{j=1}^k E_j \left[\sum_{b=j}^k \frac{1}{b(1 + \log(k/b))} + \sum_{b=1}^{j-1} \frac{1}{j(1 + \log(k/b))} \right] (1 + o(1)) \\ &\quad + Q_0(n/k) \bar{c}_{k,p}(1 + o_p(1)). \end{aligned}$$

Again, by Riemann integration we have that

$$\frac{1}{k} \sum_{b=j}^k \frac{1}{(b/k)(1 + \log(k/b))} \approx \int_{j/k}^1 \frac{du}{u(1 - \log(u))} = \log(1 + \log(k/j)),$$

and

$$\sum_{b=1}^{j-1} \frac{1}{j(1 + \log(k/b))} \approx \frac{k}{j} \int_0^{j/k} \frac{du}{1 - \log(u)} = \frac{ek}{j} \mathbf{E}(1 + \log(k/j)).$$

Similarly,

$$\begin{aligned}
\bar{c}_{k,p} &\approx \frac{1}{p} \int_0^1 \frac{(1-p)^{-1} u^{-p}}{1 - \log(u)} du - \frac{1}{p} \int_0^1 \frac{du}{1 - \log(u)} \\
(28) \quad &= \frac{e^{1-p}}{p(1-p)} \mathbf{E}(1-p) - \frac{e}{p} \mathbf{E}(1).
\end{aligned}$$

Putting the pieces together then indeed yields (18). \square

Proof of Theorem 3.3. Let us first decompose each summand by writing

$$\mathbb{E}[(T_{b,k} - \bar{T}_k)^2] = \mathbb{E}[(T_{b,k} - \xi)^2] + \mathbb{E}[(\bar{T}_k - \xi)^2] - 2 \mathbb{E}[(T_{b,k} - \xi)(\bar{T}_k - \xi)],$$

and subsequently consider each term separately. From (27) we have that

$$\mathbb{E}[(T_{b,k} - \xi)^2] = \mathbb{V}[T_{b,k}] + \text{Bias}^2[T_{b,k}] = \xi^2 \frac{\frac{1}{b} + \sum_{j=b+1}^k 1/j^2}{(1 + \sum_{j=b+1}^k j^{-1})^2} + Q_0^2(n/k) c_{b,k,p}^2 (1 + o_p(1)).$$

On the other hand, (18) gives

$$\begin{aligned}
\mathbb{E}[(\bar{T}_k - \xi)^2] &= \mathbb{V}[\bar{T}_k] + \text{Bias}^2[\bar{T}_k] \\
&= \frac{\xi^2}{k^2} \sum_{j=1}^k \left[\log(1 + \log(k/j)) + \frac{ek}{j} \mathbf{E}(1 + \log(k/j)) \right]^2 (1 + o(1)) \\
&\quad + Q_0^2(n/k) \left[\frac{e^{1-p}}{p(1-p)} \mathbf{E}(1-p) - \frac{e}{p} \mathbf{E}(1) \right]^2 (1 + o_p(1)).
\end{aligned}$$

The third term can be analyzed using both (18) and (27) as follows,

$$\begin{aligned}
\mathbb{E}[(T_{b,k} - \xi)(\bar{T}_k - \xi)] &= \mathbb{E}[(T_{b,k} - \mathbb{E}[T_{b,k}])(\bar{T}_k - \mathbb{E}[\bar{T}_k])] + Q_0^2(n/k) c_{b,k,p} \bar{c}_{k,p} \\
&= \xi^2 \mathbb{E} \left[\left(\frac{\frac{1}{b} \sum_{j=1}^b (E_j - 1) + \sum_{j=b+1}^k (E_j - 1)/j}{1 + \sum_{j=b+1}^k j^{-1}} \right) \left(\sum_{i=1}^k \frac{E_i - 1}{k} S(i, k) (1 + o(1)) \right) \right] \\
&\quad + Q_0^2(n/k) c_{b,k,p} \bar{c}_{k,p} \\
&= \xi^2 \frac{\sum_{j=1}^k (j \vee b)^{-1} S(j, k)}{k(1 + \sum_{j=b+1}^k j^{-1})} (1 + o(1)) + Q_0^2(n/k) c_{b,k,p} \bar{c}_{k,p}
\end{aligned}$$

where $S(j, k) := \log(1 + \log(k/j)) + \frac{ek}{j} \mathbf{E}(1 + \log(k/j))$.

We now proceed to add the k summands of the expected variance. To this end, some preparatory calculations will be helpful. By (17) and Riemann approximation we have

$$\begin{aligned} \frac{1}{k} \sum_{b=1}^k c_{b,k,p}^2 &\approx \frac{1}{k} \sum_{b=1}^k \frac{1}{p^2} \cdot \frac{\frac{((k+1)/b)^{2p}}{(1-p)^2} - 2\frac{((k+1)/b)^p}{1-p} + 1}{(1 + \log((k+1)/b))^2} \\ &\approx \frac{1}{p^2(1-p)^2} [1 - e^{1-2p}(1-2p)\mathbf{E}(1-2p)] \\ &\quad - \frac{2}{p^2(1-p)} [1 - e^{1-p}(1-p)\mathbf{E}(1-p)] \\ &\quad + \frac{1}{p^2} [1 - e\mathbf{E}(1)]. \end{aligned}$$

By virtue of (28),

$$\bar{c}_{k,p}^2 \approx \frac{e^{2(1-p)}}{p^2(1-p)^2} \mathbf{E}^2(1-p) - 2\frac{e^{2-p}}{p^2(1-p)} \mathbf{E}(1-p)\mathbf{E}(1) + \frac{e^2}{p^2} \mathbf{E}^2(1),$$

from which we deduce that as $k \rightarrow \infty$,

$$\frac{1}{k} \sum_{b=1}^k c_{b,k,p}^2 - \bar{c}_{k,p}^2 \rightarrow f(p),$$

where $f(p)$ is given by (19).

Observe that for the terms arising from the expected covariance term

$$\begin{aligned} \frac{1}{k} \sum_{b=1}^k \frac{\frac{1}{b} + \sum_{j=b+1}^k 1/j^2}{(1 + \sum_{j=b+1}^k j^{-1})^2} &\approx \frac{2}{k} \int_0^1 \frac{du}{u(1 - \log(u))^2} - \frac{1}{k} \int_0^1 \frac{du}{(1 - \log(u))^2} \\ &= \frac{1 + e\mathbf{E}(1)}{k}. \end{aligned}$$

Next,

$$\begin{aligned} &\frac{1}{e} \frac{1}{k} \sum_{b=1}^k \frac{\sum_{j=1}^b b^{-1}(\log(1 + \log(k/j)) + \frac{ek}{j}\mathbf{E}(1 + \log(k/j)))}{1 + \log(k/b)} \\ &\approx \int_0^1 \frac{1}{z \log(e/z)} \left(\int_0^z \frac{1}{u} \left(\int_{\log(e/u)}^\infty \log(v)e^{-v} dv \right) du \right) dz \\ &\approx 0.266 =: I_1 \end{aligned}$$

and

$$\begin{aligned} &\frac{1}{e} \frac{1}{k} \sum_{b=1}^k \frac{\sum_{j=b+1}^k j^{-1}(\log(1 + \log(k/j)) + \frac{ek}{j}\mathbf{E}(1 + \log(k/j)))}{1 + \log(k/b)} \\ &\approx \int_0^1 \frac{1}{\log(e/z)} \left(\int_z^1 \frac{1}{u^2} \left(\int_{\log(e/u)}^\infty \log(v)e^{-v} dv \right) du \right) dz \\ &\approx 0.135746 =: I_2. \end{aligned}$$

Finally, for the mean squared error term of \bar{T}_k we find

$$\begin{aligned} & \frac{1}{k} \sum_{j=1}^k (k/j)^2 \left(\int_{\log(e/u)}^{\infty} \log(v) e^{-v} dv \right)^2 \\ & \approx \int_0^1 u^{-2} \left(\int_{\log(e/u)}^{\infty} \log(v) e^{-v} dv \right)^2 du \\ & \approx 0.148005 =: I_3. \end{aligned}$$

Altogether we hence obtain

$$\begin{aligned} & \mathbb{E} \left[\frac{1}{k} \sum_{b=1}^k (T_{b,k} - \bar{T}_k)^2 \right] \\ & = \frac{1}{k} \sum_{b=1}^k (\mathbb{E}[(T_{b,k} - \xi)^2] + \mathbb{E}[(\bar{T}_k - \xi)^2] - 2 \mathbb{E}[(T_{b,k} - \xi)(\bar{T}_k - \xi)]) \\ & = \xi^2 \left(\frac{1 + e \mathbf{E}(1)}{k} \right) (1 + o(1)) + \xi^2 \frac{e^2}{k} I_3 (1 + o(1)) \\ & \quad - 2\xi^2 \frac{e}{k} (I_1 + I_2) (1 + o(1)) + Q_0^2(n/k) \left[\frac{1}{k} \sum_{b=1}^k c_{b,k,p}^2 - \bar{c}_{k,p}^2 \right] (1 + o_p(1)) \\ & = \xi^2 \left(\frac{1 + e \mathbf{E}(1)}{k} \right) (1 + o(1)) + \xi^2 \frac{e^2}{k} I_3 (1 + o(1)) \\ & \quad - 2\xi^2 \frac{e}{k} (I_1 + I_2) (1 + o(1)) + Q_0^2(n/k) f(p) (1 + o_p(1)) \\ & = \frac{C}{k} \xi^2 (1 + o(1)) + Q_0^2(n/k) f(p) (1 + o_p(1)) \end{aligned}$$

with

$$C = 1 + e \mathbf{E}(1) + e^2 I_3 - 2e(I_1 + I_2) \approx 0.502727.$$

□